An investigation on the origin of regional spring time ozone episodes in the Western Mediterranean

Pavlos Kalabokas[1,2], Jens Hjorth[2], Gilles Foret[3], Gaëlle Dufour[3], Maxim Eremenko[3], Guillaume Siour[3], Juan Cuesta[3], Matthias Beekmann[3]

[1]Academy of Athens, Research Center for Atmospheric Physics and Climatology, Athens, Greece

[2]European Commission, Joint Research Centre (JRC), Institute for Environment and Sustainability (IES), Air and Climate Unit, I - 21027 Ispra (VA), Italy

[3]Laboratoire Inter-universitaire des Systèmes Atmosphériques (LISA), Universités Paris-Est Créteil et Paris Diderot, CNRS, Créteil, France

Correspondence to: Pavlos Kalabokas (pkalabokas@academyofathens.gr)

Abstract. For the identification of regional spring time ozone episodes, rural EMEP ozone measurements from countries surrounding the Western Mediterranean (Spain, France, Switzerland, Italy, Malta) have been examined with emphasis on periods of high ozone mixing ratios, according to the variation of the daily afternoon (12:00 – 18:00) ozone values. For two selected high ozone episodes in April and May 2008, composite NCEP/NCAR reanalysis maps of various meteorological parameters and/or their anomalies (geopotential height, specific humidity, vertical wind velocity omega, vector wind speed and temperature) at various tropospheric pressure levels have been examined together with the corresponding satellite IASI ozone measurements (at 3 and 10 km), CHIMERE simulations, vertical ozone soundings and HYSPLIT back trajectories. The observations show that high ozone values are detected in several countries simultaneously over several days. Also, the examined spring ozone episodes over the Western Mediterranean and in Central Europe are linked to synoptic meteorological conditions very similar to those recently observed in summertime ozone episodes over the Eastern Mediterranean (Kalabokas et al., 2013; Doche et al., 2014; Kalabokas et al., 2015), where the transport of tropospheric ozone-rich air masses through atmospheric subsidence influences significantly the boundary layer and surface ozone mixing ratios. In particular, the geographic areas with observed tropospheric subsidence seem to be the transition regions between high pressure and low pressure systems. During the surface ozone episodes IASI satellite measurements show extended areas of high ozone in the lower and upper troposphere over the low pressure system areas, adjacent to the anticyclones, which influence significantly the boundary layer and surface ozone mixing ratios within the anticyclones by subsidence and advection in addition to the photochemically produced ozone there, resulting in exceedances of the 60 ppb standard.

1 Introduction

Surface ozone is a pollutant harmful to both human health and vegetation (Levy et al., 2001; Fuhrer, 2009). Further, in the upper troposphere ozone acts as a powerful greenhouse gas (IPCC, 2007). The mixing ratios of ozone throughout the troposphere depend on the meteorological conditions driving vertical and horizontal transport and on photochemical ozone production from its precursors, nitrogen oxides (NO_x) volatile organic

compounds (VOCs) and carbon monoxide (Delmas et al., 2005; Seinfeld and Pandis, 2006; Monks et al., 2015). Recent model studies and studies based on observational constraints indicate that a little less than 90% of the ozone found in the troposphere is formed photochemically within the troposphere, the remaining part is brought down to the troposphere by stratosphere-troposphere exchange (Monks et al., 2015).

The European network of surface ozone monitoring stations shows persistently exceedances of the European long-term target value for protection of human health, under anticyclonic synoptic meteorological conditions during the warm season in southern and central Europe (EEA, 2015). The Mediterranean area is particularly exposed to ozone pollution because of the combination of the specific meteorological conditions prevailing during spring and summer and the regional air pollutant emissions. Data collected from air pollution monitoring stations in combination with results of measurement campaigns show that ozone mixing ratios in the Mediterranean Basin are relatively high: Lelieveld et al. (2002) found that summer ozone mixing ratios over the Mediterranean are a factor of 2.5–3 higher than in the hemispheric background troposphere, in the boundary layer and up to 4 km altitude. Rural stations in continental Greece, Italy, Malta and eastern Spain report summer average ozone values of about 60–70 ppb, significantly higher than values in Northern and Western Europe (Bonasoni et al., 2000; Kalabokas et al., 2000; Millan et al., 2000; Kourtidis et al., 2002; Kouvarakis et al., 2002; Nolle et al., 2002; Kalabokas and Repapis, 2004; Paoletti, 2006; Sánchez et al., 2008; Schürmann et al., 2009; Velchev et al., 2011, Kalabokas et al., 2008; Kleanthous et al., 2014; Cristofanelli et al., 2015). Results from 3-D chemistry transport models also suggest that ozone mixing ratios are higher than for the rest of Europe (e.g. Johnson et al., 2001). High ozone values in the Mediterranean are typical not only for ground level measurements, but for the entire boundary layer as well as the entire lower troposphere (Millan et al., 1997, 2000; Kalabokas et al., 2007).

The Mediterranean climate with frequent anticylonic, clear sky conditions in spring and summer favours photochemical ozone formation in the troposphere. Furthermore, Mediterranean tropospheric ozone levels are influenced by long-range transport of ozone and its precursors from Europe, Asia and even North America as well as emissions of precursors from sources around the Basin, particularly the large cities (Lelieveld et al., 2002, Gerasopoulos, 2005, Safieddine et al., 2014). Also natural VOC emissions in the area have been found to be important ozone precursors (Richards et al., 2013). Several studies in the Western part of the Mediterranean involving measurements as well as model simulations (e.g. Millan et al., 1997, 2000, Querol et al. 2016) have addressed the causes of episodes with high ozone mixing ratios. It was found that the typical synoptic meteorological conditions found during the summer in this part of the Mediterranean, with a lack of strong synoptic advection combined with the orographic characteristics and the sea and land breezes favour episodes where high levels of ozone are accumulated by recirculation of air masses loaded with ozone precursors.

Anticyclones are generally linked to atmospheric subsidence, which seems to be particularly important over the Eastern Mediterranean as a cause of elevated ozone mixing ratios. During the summer period, the Mediterranean area is directly under the descending branch of the Hadley circulation, caused by deep convection in the tropics (Lelieveld, 2009). However a main reason for the strong subsidence observed in the Mediterranean Basin appears to be an impact of the Indian monsoon, inducing a Rossby wave that by the interaction with the midlatitude westerlies produces adiabatic descent in the area (Rodwell and Hoskins, 1996, 2001; Tyrlis et al., 2013). In general, in the Eastern Mediterranean strong deep subsidence in the lower troposphere influencing the

boundary layer has been documented, based essentially on the analysis of MOZAIC vertical ozone profiles as well as surface ozone and satellite measurements (Kalabokas et al., 2007; Kalabokas et al., 2008; Eremenko et al, 2008; Foret et al., 2009; Liu et al., 2009; Kalabokas et al., 2013; Doche et al., 2014; Kalabokas et al., 2015). Also data analysis based on large-scale atmospheric modeling studies (Li et al, 2001; Richards et al., 2013; Zanis et al., 2014; Safieddine et al., 2014; Tyrlis et al., 2014) shows the importance of vertical transport of ozone in the Mediterranean area, particularly in its eastern part.

Recent research based on vertical MOZAIC ozone profiles (Kalabokas et al., 2015) suggests that during days with the highest ozone levels for both the free lower troposphere (1.5-5 km) and the boundary layer (0-1.5 km) over the middle-eastern airports of Cairo and Tel-Aviv there are extended regions of strong subsidence in the Eastern Mediterranean but also in Eastern and Northern Europe and over these regions the atmosphere is dryer than average.

The influence of tropospheric transport of ozone at hemispheric scale, on surface ozone mixing ratios, is an issue of potential importance to ozone abatement policies. Vertical transport of ozone is of particular relevance to the ozone transport over long distances in the troposphere because the lifetime of ozone in the free troposphere is longer so it can be transported over longer distances than in the boundary layer (HTAP, 2010). The impact on surface ozone of the long range transport of ozone has been extensively investigated in the US, where a clear difference has been observed between the eastern part, where surface ozone mixing ratios have decreased very significantly, and the western part, where most sites do not show such a trend, apparently due to the effects of transport (Cooper et al., 2012). Studies based on observations and trajectory modelling indicate that transport above the boundary layer and entrainment of ozone from the free troposphere has an important impact on surface ozone mixing ratios at several sites in the western US (Cooper et al., 2011; Langford et al., 2015). Also a changing seasonal cycle of ozone, with a tendency towards a maximum earlier in the year, has been tentatively explained by the influence of atmospheric transport patterns combined with a change in the temporal and spatial emissions of ozone precursors (Parrish et al., 2013).

The importance of hemispheric transport for Mediterranean air pollution in particular has previously been highlighted in the modelling study by Stohl et al. (2002) of intercontinental transport of air pollutants, who found the highest mixing ratios of a passive tracer for North American emissions in the Mediterranean Basin. The modelling studies of Richard et al. (2013) and Safieddine et al. (2014) both come to the conclusion that the emission sources within the Mediterranean area have a dominating influence on surface ozone while remote sources, e.g. in Asia and North America, are more important than local sources for ozone mixing ratios at higher altitudes (above 700 hPa according to Richards et al. 2013). The radiative (climate) impact of ozone depends mainly on the mixing ratios above the boundary layer. Relatively high ozone mixing ratios are reported in the Central Mediterranean also during the winter-early spring period (Nolle et al., 2002) while, in an extended observational study in the Western Mediterranean basin a converging trend between the background rural ozone values and the urban ozone values was reported (Sicard et al., 2013).

Many studies of Mediterranean ozone have been focused on the Eastern part of the Mediterranean basin where the influence of downwards transport appears to be more important than it is in the Central and Western part, although also at this part of the Mediterranean very frequently anticyclonic conditions dominate in spring and

summer months. The mechanisms governing ozone levels in the Western and Central Mediterranean appear to need further clarification particularly regarding the conditions during springtime. For example, in Kalabokas et al. (2008) as well as in the more recent study by Zanis et al. (2014) it was found that rural background ozone monitoring stations in the Western and Central Mediterranean show climatological spring time ozone maximum in April-May while the corresponding rural background ozone Eastern Mediterranean stations, have their climatological maxima in July-August. Also, in Eastern Greece and the Aegean Sea the summer rural background ozone levels are systematically higher than the corresponding ones observed in the Central Mediterranean (Malta) and the Eastern Mediterranean (Cyprus). The above is contrary to the predictions of a model simulation that suggested a rather uniform ozone distribution across the basin (Zanis et al., 2014). Understanding the origin of high ozone levels during spring time is particularly challenging because this is a period where photochemical formation in the troposphere is increasing due to rising sun intensity, but also stratospheric intrusions may be of relevance as these have been found to have a maximum in Southern Europe in spring/early summer (Beekmann et al., 1994; Monks, 2000).

The focus of the present study thus is to improve the understanding of ozone behaviour over the Western Mediterranean and the surrounding area to the north part of the basin, towards central Europe in the springtime. In particular, it aims at investigating to which extend surface ozone mixing ratios during the high ozone episodes are influenced by entrainment of ozone rich air. Further, this study investigates the factors controlling ozone distribution in the free troposphere, particularly transport within the troposphere, stratosphere-troposphere exchange and photochemical formation in the free troposphere. Two episodes in late April and early May have been selected for a detailed analysis. We analyze the two spring time episodes of high surface ozone mixing ratios over the Western Mediterranean and the surrounding area using a comprehensive combination of surface observations, Infrared Atmospheric Sounding Interferometer (IASI) satellite observations, meteorological maps, back trajectories and regional air quality modelling to understand the principal mechanisms contributing to these events.

2   Data and methodology

The following data will be used in the analysis:

1) Ozone measurements from the European Monitoring and Evaluation Programme (EMEP) and European Environment Agency (EEA) air pollution network

The surface ozone measurements during spring 2008 (March-May) of some EMEP (EMEP, 2015) rural ozone stations (http://www.nilu.no/projects/ccc/onlinedata/ozone/) surrounding the western Mediterranean basin [Spain, Cabo de Creus (ES10, 42.31 ^{o}N, 3.31 ^{o}E), France, Morvan (FR10, 47.26 ^{o}N, 4.08 ^{o}E) and Montandon (FR14, 47.30 ^{o}N, 6.83 ^{o}E), Switzerland, Payerne (CH02, 46.81 ^{o}N, 6.94 ^{o}E) and Chaumont (CH04, 47.04 ^{o}N, 6.97 ^{o}E), Italy, Montelibretti (IT01, 42.10 ^{o}N, 12.63 ^{o}E) and Ispra (IT04, 45.80 ^{o}N, 8.63 ^{o}E), Malta, Giordan Lighthouse (MT01, 36.07 ^{o}N, 14.21 ^{o}E)] have been analyzed with emphasis on periods of high ozone, focused mostly on the day-to-day variations of the mean afternoon (12:00 – 18:00) ozone values. In addition, during the selected spring ozone episodes the measurements of the EEA air pollution network are also taken into account for the analysis (EEA, 2015).

2) Composite NOAA/ESRL and ECMWF Reanalysis maps

Composite or daily NOAA/ESRL and ECMWF reanalysis meteorological maps covering Europe and N. Africa and corresponding to periods of high ozone have been plotted for the following meteorological parameters: Geopotential height, specific humidity anomaly, vertical wind velocity Omega (and anomaly), vector wind speed and temperature anomaly. The examination was focused on the tropospheric pressure levels at 850, 700 and 500hPa levels (for space limitations mainly the 850hPa charts are presented). The NOAA/ESRL charts are based on grids of 2.5×2.5 degrees, following the procedure of Kalnay et al. (1996) while the horizontal resolution of ECMWF charts is 0.25× 0.25 degrees.

3). HYSPLIT back trajectories

Six-day back trajectories were calculated with end points at 50, 500 and 1500 meter altitude, using the NOAA HYSPLIT model with GDAS meteorological data (Draxler and Rolph, 2015) for the EMEP stations and the days of the selected ozone episodes. The GDAS data have a horizontal resolution of 1 degree and 23 vertical levels between 1000 and 20 hPa.

4). Satellite IASI ozone measurements

Satellite observations provide interesting possibilities to support the analysis of ground measurements as well as modeling simulations. Indeed, during the last decade, satellite observations of tropospheric ozone have been developed and have become more and more precise (e.g. Fishman et al., 2003; Liu et al., 2005; Coheur et al., 2005; Worden et al., 2007; Eremenko et al., 2008). These observations are now able to complement in situ observations, offering wide spatial coverage and good horizontal resolution.

The IASI instrument (Clerbaux et al., 2009), on board the MetOp-A platform since 19 October 2006, is a nadir-viewing Fourier transform spectrometer operating in the thermal infrared between 645 and 2760 cm^{-1} with an apodized spectral resolution of 0.5 cm^{-1}. The IASI field of view is composed of a 2×2 matrix of pixels with a diameter at nadir of 12 km each. IASI scans the atmosphere with a swath width of 2200 km, allowing the monitoring of atmospheric composition twice a day at any (cloud-free) location. The spectral coverage and the radiometric and spectral performances of IASI allow this instrument to measure the global distribution of several important atmospheric trace gases (e.g. Boynard et al., 2009; George et al., 2009; Clarisse et al., 2011). As in Doche et al. (2014), IASI data at 3 and 10 km height are used here for analysis. These levels are representative for the lower and upper troposphere respectively. However, due to the limited vertical sensitivity and resolution of IASI, ozone mixing ratios retrieved at 3 km describe the ozone variability from roughly 2 to 8 km, and ozone mixing ratios retrieved at 10 km describe the ozone variability from 5 to 14 km (Dufour et al., 2010). Despite this overlapping, recent studies show that uncorrelated information from the lower and the upper troposphere can be derived from IASI (Dufour et al., 2010, 2012, 2015).

5) Vertical ozone soundings

Further information about the vertical ozone distribution is obtained from the ozone soundings made from the site of Payerne, Switzerland, Uccle, Belgium and Hohenpeissenberg, Germany. These are regularly carried out with balloon launches starting at 11 AM UTC using ECC (Electrochemical Mixing ratio Cell) ozonesondes in Payerne and Uccle and Brewer-Mast ozonesondes in Hohenpeissenberg. The data were downloaded from the

website of the World Ozone and Ultraviolet Data Centre (WOUDC, 2015), uncertainties on the measured ozone mixing ratios for ECC ozonesondes are between 5 and 10% (Rene Stübi, personal communication).

6). Regional air quality simulations

The CHIMERE model (Menut et al, 2013) is a state-of-the-art model widely used for pollution and air quality studies (Rouil et al., 2009; Beekmann and Vautard, 2010). For the purpose of this study, we have used a version of the model covering a western European domain (35° N – 70° N latitude, 15° W - 35° E longitude). The whole troposphere is described from ground to about 200 hPa using 30 hybrid (sigma, P) levels. The meteorological forcing is given by the IFS forecast of the ECMWF based each day on the 0 and 12 am analysis. The anthropogenic emissions are prescribed by using the TNO inventory (Kuenen et al, 2014) while natural emissions are calculated by the MEGAN module (Guenther et al, 2006). A passive tracer has been used to analyse the dynamics patterns responsible for ozone transport, which is initialized and emitted in the top model layer (11-12 km) i.e within the upper troposphere every hour. A 10- day period (spin-up period) is simulated before each targeted period to establish a kind of equilibrium state of the tracer. Moreover, simulations have also been made by switching off emissions for both periods under study. A difference between simulations with and without emissions is a proxy of the photochemical production of ozone within the boundary layer. The current configuration of the CHIMERE model uses a horizontal resolution of 0.25° x 0.25° and 30 hybrid (σ,p) vertical levels are used to describe the whole troposphere (i.e from the ground to 200hPa).

The methodology used in this paper is the following:

At first, in order to minimize local pollution effects and focus on boundary layer ozone measurements representative of a wider geographical area than the station location, only the afternoon (12:00 – 18:00) ozone mixing ratios, typically representing a well-mixed boundary layer, have been analyzed.

Also, recent observations over the Mediterranean both from MOZAIC tropospheric ozone profiles (Kalabokas et al., 2013) as well as satellite data (Zanis et al., 2014) show a strong anticorrelation between ozone and atmospheric humidity. Therefore, in dry and descending air masses originating from the upper tropospheric layers, higher tropospheric ozone levels would be expected. It is well known that the mixing ratio of water vapour in the troposphere (specific humidity) tends to decrease with increasing altitude because the lower air temperatures at higher altitudes cause elimination of water vapour by condensation followed by precipitation. This makes specific humidity an indicator of subsiding air masses, which will be used in the analysis.

In addition, previous research carried out in the Mediterranean (Kalabokas et al., 2007; Kalabokas et al., 2008; Velchev et al., 2011; Kalabokas et al., 2013; Kalabokas et al., 2015) suggested that there is a strong link between synoptic meteorology conditions and ozone mixing ratio variability.

Based on the above, a systematic investigation of the composite meteorological maps during two spring high ozone episodes at the 850 hPa pressure level was carried out, until 5 days before the event for the meteorological parameters mentioned previously. The purpose of the analysis is to identify areas of high subsidence in the free troposphere, which could potentially influence the examined surface ozone measurements, considering also that the afternoon (12:00 – 18:00) ozone mixing ratios are quite representative of the boundary layer values. The high subsidence areas were detected in the first place by the positive vertical velocity omega (and anomalies) as well

as the negative specific humidity anomalies. Also, the geographical distributions of geopotential heights, temperature anomalies and vector wind speed were very useful in the examination of the influence of synoptic meteorological conditions on ozone mixing ratios. In addition, air mass back trajectories (NOAA HYSPLIT), satellite IASI ozone measurements at the 3km and 10km levels, afternoon surface ozone measurements from the EEA European network and vertical ozone profile measurements in Central Europe during a selected ozone episode, were used for the analysis. Finally, CHIMERE tracer simulations and modelling of ozone field for the April and May 2008 ozone episodes have been performed for the validation of the analysis of measurement data. The satellite tropospheric ozone measurements are used to monitor the movement of the high tropospheric ozone reservoirs and their potential influence to the boundary layer.

3 Results and discussion

3.1 Surface Ozone measurements in the Western Mediterranean basin in spring 2008

In Fig. 1 (upper panel) the afternoon (12:00 – 18:00) rural ozone mixing ratios of selected EMEP stations from countries surrounding the Western Mediterranean basin (Spain, France, Switzerland, Italy, Malta) during spring (March – May) 2008 have been plotted. A first investigation of the plots leads to the following remarks:

a). Episodic periods of high ozone (and also for low ozone) may last for several days and they can be detected simultaneously in many countries surrounding the western Mediterranean basin.

b). The 60 ppb (120 μg/m^3) EU standard for human health protection can be exceeded over many days and in many countries.

From the above stations, the ozone mixing ratios measured at the EMEP stations in France and Switzerland as well as the EMEP station in Northern Italy (IT04, JRC-Ispra), presented in Fig. 1 (lower panel), show generally a very good agreement between each other. This feature is remarkable given their different site characteristics, the large distance between them as well as their location relative to the huge natural barrier of the Alpine mountainous area. So, the high mid-day ozone mixing ratios observed simultaneously over many countries could be considered as regional ozone episodes. The two regional spring 2008 ozone episodes with the highest ozone mixing ratios in the examined area were on 26-27 April, 2008 and 7-9 May, 2008; they have been selected for further analysis.

3.2 Geographical distribution of meteorological parameters, IASI tropospheric ozone measurements and CHIMERE modelling tracer simulations during the April 26-27, 2008 ozone episode

The composite NOAA/ESRL Reanalysis maps of geopotential height, vertical velocity omega, vector wind speed, temperature anomaly and specific humidity anomaly at 850 hPa as well as IASI satellite ozone mixing ratios for the high ozone episode of April 26-27, 2008 are presented in Fig. 2, while the corresponding composite maps for 2, 3 and 5 days before the episode, are shown in Figs I-III of the Annex. In addition, the corresponding ECMWF charts at 900hPa and 800hPa for geopotential height, vertical velocity omega and vector wind speed

are shown in Fig. 3. The corresponding composite maps at the 700hPa and 500 hPa pressure levels have also been plotted and analyzed (not shown). The examination of these meteorological charts leads to the following remarks:

a). The anticyclone located to the west of the N. African coast is progressively strengthening and expanding after April 23-24, 2008 while moving rapidly towards the European continent. At the same time the low pressure system installed over E. Europe on April 21-24 is progressively reduced to a cut-off low on April 26-27 while moving towards Greece and Turkey.

b). Negative specific humidity anomalies are observed all over N. and E. Europe as well as over the Atlantic Ocean while at the peak of the episode (April 26-27) the dry air masses prevail over a vast and extended area from Russia to NW Africa and the Atlantic.

c). An extended area of positive vertical velocity omega (and anomalies), which is a direct sign of subsiding air masses, is observed over the W. Mediterranean and the Atlantic and is moving rapidly towards the Central Mediterranean. Five days before the episode (April 21-22) the maximum of subsidence area was observed over the Iberian Peninsula and the adjacent ocean up to the Canary islands. Then it is moving rapidly eastwards, showing a maximum over Italy at the peak of the episode (April 26-27) as well as a secondary maximum over Germany. The positive omega anomalies indicate that the observed subsidence during the episode days is higher than usual for this period of the year and the examined geographical regions.

d). A strong westerly flow is observed over the Western Mediterranean region of subsidence with the air masses originating from the region of N. Atlantic where a deep and extended low pressure system is observed. As seen, the extension of the N. African anticyclone towards the Western Mediterranean changes progressively the very strong westerly flow (observed 5 days before the episode, April 21-22) to a strong north-westerly. Also, strong N-NW winds over the Central Mediterranean prevail at the interface area between the cut-off low and the anticyclone.

e). Strong and extended negative temperature anomalies are observed 5 days before the episode over the Iberian peninsula and the adjacent N. African coast, moving towards the Central Mediterranean and the Libyan coast. The negative temperature anomaly area becomes more extended during the episode days, indicating that colder atmospheric conditions than the normal prevail during the ozone episode over the corresponding areas, while during photochemical ozone episodes higher than normal air temperatures would be expected. This can be explained as an impact of transport of cold air masses to these areas.

Overall, over the same area of subsidence, strong winds together with positive omega vertical velocity (and anomalies) are observed as well as negative humidity anomalies, thus indicating a strong descending air current, which transports rapidly tropospheric air towards the boundary layer.

In Figure 1, the composite IASI satellite ozone mixing ratios at 3km for April 26-27, 2008 are presented as well, while in Fig. IV of the Annex, the composite ozone IASI measurements from April 21, 2008 to April 27, 2008 at two altitude levels (3 km and 10 km), which are considered representative for the lower and the upper troposphere (Doche et al., 2014) , even if a partial overlap occurs due to reduced resolution (see section 2), are also shown. An extended area of very high ozone in the upper and lower troposphere is observed over the N.

Atlantic over the area covered by the low pressure system. At the same time, in the Central Mediterranean a high tropospheric ozone area is progressively formed at both examined tropospheric layers (3 and 10 km) and having its maximum on April 26-27. This observation could be associated with the information extracted from the analysis of the composite meteorological charts over this Central Mediterranean area where clear indications of very strong subsidence of dry air masses is observed together with very strong north-westerly winds recorded over the Mediterranean at 850hPa (Fig. 1 and Annex Figs I-III), especially for April 26-27. The same features are also observed at the pressure levels of 700hPa and 500 hPa (not shown).

For a more detailed analysis during the maximum of the episode (April 26-27), in Fig. 4 the daily IASI satellite ozone measurements at 3 and 10 km altitude are presented in a higher mixing ratio resolution as well as in a more restricted geographical domain (same as the CHIMERE simulation outputs), where the above described characteristics of the geographical distribution of tropospheric ozone appear more clear. Also, for a more detailed investigation of the corresponding meteorological characteristics at higher tropospheric levels, in Annex Fig. V the daily meteorological charts of columnar precipitable water anomaly and geopotential heights at 500hPa and 700hPa for April 26 and 27, 2008 are presented. The very extended areas with negative columnar precipitable water anomalies show that the dry conditions, indicating subsidence, prevail over the whole troposphere, mostly over its lower part, over a vast area and especially at the interface areas of the high and low pressure systems at 500 hPa, very similar to what was already observed at 850 hPa (Fig. 2). So, it comes out that during the ozone episode the same synoptic pattern is observed in the troposphere up to 500 hPa (Annex Fig. V) but even at higher levels (not shown). Also in Fig. 3, the graphical representation on the map of the daily evolution of the hourly surface ozone mixing ratios at 15:00 h as recorded in the air pollution stations of the EEA-AirBase network (EEA, 2015) for 26-27 April shows very high mixing ratios, exceeding 70 ppb, appearing at many locations in Spain as well as in S. France and NW Italy. As mentioned previously, during the afternoon hours the influence of the free troposphere on the boundary layer is maximized through vertical mixing, and the composite meteorological maps show a large corridor of subsiding dry air masses over the same area (Fig. 1, Annex Figs I-III), which is a very strong indication that the surface ozone mixing ratios could be influenced by entrainment of subsiding ozone-rich air. Obviously, the distribution of ozone mixing ratios measured at the ground level stations show important differences from those observed at 3 km height (Fig. 3), as expected, due to the barrier, caused by the temperature inversion, between the boundary layer and the free troposphere and the importance of photochemical formation and transport of ozone within the boundary layer, where the precursor mixing ratios are relatively high.

In order to study in more detail the atmospheric processes prevailing during the examined April ozone episode and complete the analysis of the dynamic atmospheric conditions during the examined events, regarding more specifically the origin of ozone measured in the boundary layer, we have performed simulations with the CHIMERE model using tracers to analyze transport patterns. The results of the CHIMERE simulations for the April episode are shown in Fig. 5, where simulations of the ozone field (together with the iso-contours of the high tropospheric tracer) are presented. Also, in Annex Fig. VI simulations of upper tropospheric tracer mixing ratios and simulations of photochemical ozone production are shown. As described earlier (cf Chapter 2), we use a tracer initialized within the model top layer in the upper troposphere at about 11 km height. Inspecting qualitatively simulated mixing ratios at 3 km and 1.5 km altitude (Fig. 5), it is shown that the upper tropospheric

tracer is present at these levels, indicating significant downward transport of upper troposphere air masses to the boundary layer, which coincides with the maximum mixing ratios of the CHIMERE simulated ozone field at 3 and 1.5 km covering a large area from Switzerland to Malta (Fig. 5). Combining that with the meteorological charts (Fig. 2), on the outer side of the low-pressure area and at the interface with the N. African anticyclone high values of the upper tropospheric tracer indicating considerable subsidence are observed at 5 km altitude (not shown), which becomes even stronger and more extended at the 3 km and 1.5 km altitudes (Fig.5). So, following the geographical distribution of the upper tropospheric tracer at 3 km and 1.5 km (Fig.5), tropospheric subsidence is observed at the periphery of the anticyclonic area and at the interface with the low-pressure area. Therefore, the downward transport of upper tropospheric ozone is influencing the boundary layer over the examined location. The observed patterns, based on CHIMERE tracer simulations and on ozone mixing ratios are quite consistent with the observed values of the IASI instrument that show the same structures (Figs 2,4), as well as with the analysis of meteorological parameters based on composite charts (Fig. 2) and described above. Regarding the comparison of the geographical distribution of the CHIMERE ozone field (Fig. 5) with the IASI measurements at 3 km or 700hPa (Figs 2, 4), a clear difference over the N. Atlantic and also differences over the Ionian Sea and the Aegean Sea are observed. As discussed above, over these regions the prevailing low pressure systems, inducing lower tropopause heights, are associated with high tropospheric ozone levels. It has to be mentioned that direct comparison of CHIMERE simulations at 3 km with the corresponding IASI measurements presents some weaknesses, especially due to the fact that IASI is sensitive to a height range between 2 and 8 km and the IASI averaging kernels need to be applied to CHIMERE to make it comparable with IASI (Eremenko et al., 2008).

The HYSPLIT back-trajectories during the April episode arriving at the EMEP stations in Italy (JRC-Ispra) and on Malta (Fig. 6) show in fact subsiding air masses arriving from northern directions, on April 25 and 26 for Ispra and on April 27 for Malta and give more or less the same picture as the Swiss stations (not shown).

The combination of the information from the composite meteorological maps (Fig 2) and the HYSPLIT back-trajectories for the April episode (Fig. 6) shows that the prevailing NW wind during the days preceding the episode passed over the N. Atlantic region, where the IASI satellite detects a high ozone area extended throughout the whole troposphere (Figs 2, 4), which beyond any doubt contributes to the high surface ozone values. So, tropospheric transport of air rich in ozone from northern directions is likely to give an important contribution to the high surface ozone levels through the processes of advection and subsidence.

It should be noticed at this point that the interpretation of the back trajectory information is much more efficient if it is done in combination with the examination of the composite meteorological charts (and ideally satellite ozone measurements and modelling simulations). In this way the influence from areas with strong tropospheric subsidence and low atmospheric humidity (indicating high ozone) at the various tropospheric pressure levels could be easier assessed.

In summary, the April 26-27, 2008 ozone episode could be considered as a clear case of the tropospheric influence to the boundary layer through ozone transport, which is added to the photochemically produced boundary layer ozone. The analysis of meteorological charts at various tropospheric pressure levels helps in understanding that the strong subsidence occurring over the central Mediterranean plays a key role in explaining

this surface ozone episode on April 26-27, 2008. The IASI observations of lower and upper tropospheric ozone, helps in understanding that the subsidence of ozone-rich air masses characterizes this surface ozone episode. The evolution of the above described phenomenon can be effectively monitored by examining the composite meteorological maps at 850hPa during the episode days (as well as at 5-days, 3-days and 2-days before the episode, Annex Figs I-III). As mentioned, the examination of the 700hPa and 500hPa pressure levels (not shown) gives comparable results.

Based on the above results, the simultaneous strengthening and expansion of the African anticyclone and the formation of a cut-off low over the SE Balkans during the episode seem to give rise to the large scale subsidence, inducing a strong downward transport of cold air masses over the western Mediterranean and the surrounding areas while the maximum intensity of the phenomenon is observed in the geographical area located between the two synoptic atmospheric systems. As mentioned, the signs of stronger tropospheric subsidence during the episode days can be clearly observed from the negative specific humidity anomalies as well as the negative columnar precipitable water anomalies associated with positive omega anomalies (downward motion). The evolution of the temperature anomaly is interesting as the growing region of negative temperature anomaly over more or less the region of subsidence (mostly to its west) as the episode develops, could be explained by the descend of colder air from the upper tropospheric layers, transported from more northerly latitudes, caused by the interaction of the low pressure system (located to the east) and the anticyclone (located to the west). This is also consistent with the descent of upper tropospheric tracers simulated with the CHIMERE model. All the above features accompanying a situation with deep subsidence appear in all examined pressure levels at 850 hPa, 700hPa and 500 hPa.

3.3 Geographical distribution of meteorological parameters, IASI tropospheric ozone measurements and CHIMERE modelling tracer simulations during the May 7-9, 2008 ozone episode

As it will be shown in the next paragraphs, the examination of the May 7-9, 2008 episode leads to comparable remarks regarding synoptic meteorology and geographical distribution of meteorological parameters with the April episode, although in the May episode the meteorological systems and especially the anticyclone are located further to the north. In Figure 7 the composite NOAA/ESRL Reanalysis maps at 850 hPa and IASI measurements at 3 km for the high ozone episode of May 7-9, 2008 are presented. The corresponding composite charts at 850 hPa for 2, 3 and 5 days before the episode are presented in Annex Figs VII-X. In addition, the corresponding ECMWF charts at 900hPa and 800hPa for geopotential height, wind speed and vertical velocity are shown in Fig. 8. Also, the same plots for the 700 hPa, 500 hPa and 300 hPa level have been also created (not shown). The examination of all above plots gives the following:

a). A deep and extended low is located over N. Atlantic while a strong anticyclone prevails over N. Europe, centered between Great Britain and Scandinavia. At the same time deep and extended low-pressure systems over the Polar Regions and E. Europe are formed, associated with very dry conditions observed throughout the whole troposphere (Fig. 7).

b). Over a part of the anticyclonic area and especially at the region of interface of the anticyclone with the low pressure systems to the east, an extended area of positive vertical velocity omega (and anomalies) is observed, associated also with extended areas of low-humidity air masses (Fig. 7), which are clear signs of strong subsidence lasting for many days. The signs of subsidence are particularly strong also at the higher tropospheric pressure levels up to 300hPa (not shown) indicating the occurrence of a large-scale tropospheric phenomenon.

c). A strong contrast is observed (Fig. 7) between positive and negative temperature anomalies in W. and E. Europe respectively (and also geopotential height anomalies, not shown), which is similar to what has been observed for the April episode, showing strong influence of transport of air masses.

d). Stagnant conditions are observed at the center of the N. European anticyclone located over the North Sea while at the southern part of the anticyclone a strong positive vertical omega velocity is observed (indicating subsidence), which is associated with a stronger vector wind velocity over C. Europe. In fact, a strong air current starting from the N. Atlantic makes a circular clockwise motion at the periphery of the anticyclone towards the East while the flow at the northern and the western periphery of the anticyclone is particularly strengthened (Fig. 7-8, Annex Figs VII-IX). Similar features are also observed at the higher pressure levels (700hPa, 500 hPa, Annex Figs XI) as it was also the case for the April episode.

The IASI measurements (composite charts) at 3 km during the May 7-9, 2008 episode is shown in Fig. 7, while for the lower and the upper troposphere (3 and 10km respectively) for the previous 2, 3 and 5 days are shown in Annex Fig. X. During the May episode a high ozone area is observed in the lower and upper troposphere over the N. Atlantic, which is more extended during the days preceding the episode peak.

As observed (Fig. 7, Annex Fig. X) the days before the episode and over the region covered by the anticyclone, the mixing ratios of ozone in the upper troposphere (at 10 km) decrease, while the IASI measurements in the lower troposphere (at 3 km) over central Europe show a small but geographically extended increase. It has to be reminded that this phenomenon takes place exactly over the area where intense subsidence and low humidity conditions have been detected, which could be considered as a direct independent evidence of the influence of ozone mixing ratios from the upper troposphere, as it has been described and discussed in the previous paragraphs. As also seen in Figure 7, over E. Europe and Russia a significant tropospheric ozone accumulation occurs while a prevailing easterly flow from these high ozone areas is moving towards central and W. Europe. It should be reminded that over central Europe extended strong subsidence associated with dry conditions and a strong gradient of temperature anomalies are observed at the same time (Fig. 7, Annex Figs VII-X).

The above features are more clearly shown in Fig. 9 where the daily IASI satellite ozone measurements at 3 and 10 km level for the May 2008 episode are presented in a higher mixing ratio resolution as well as in a more restricted geographical domain (same as the CHIMERE model outputs) while the corresponding daily meteorological charts of columnar precipitable water anomaly and geopotential heights at 500hPa and 700hPa are shown in Annex Fig. XI. In fact, an extended region of negative columnar precipitable water anomalies (dry conditions throughout the troposphere, indicating subsidence), prevailing over a vast area covering eastern and central Europe is observed. As also seen in the April episode, this feature appears at the interface areas of the high and low pressure systems while the same synoptic patterns occur at all examined tropospheric levels. In addition, in Fig. 9 the graphical representation on the map of the daily evolution of the hourly surface ozone

mixing ratios at 15:00 h as recorded in the air pollution stations of the EEA-AirBase network (EEA, 2015) during the 7-9 May period shows very high mixing ratios, exceeding 70 ppb, appearing simultaneously at many locations from N. Italy to the British islands.

The results of the CHIMERE simulations for the May episode are shown in Fig. 10 and Annex Fig. XII, where simulations of upper tropospheric tracer mixing ratios, simulations of photochemical production and simulations of the ozone field (together with the iso-contours of the high tropospheric tracer) are presented. As described earlier (cf Chapter 2), we use one tracer initialized within the model top layer in the upper troposphere at about 11 km height. Inspecting qualitatively simulated mixing ratios at 3 km and 1.5 km altitude (Fig. 10, Annex Fig. XII), it appears that the upper tropospheric tracer is clearly detected at these levels, indicating downward transport from the upper troposphere to the boundary layer. Also in Fig. 10, the CHIMERE simulations of the ozone fields at 3 km and 1.5 km altitudes (corresponding to 700hPa and 850hPa pressure levels respectively) show high ozone mixing ratios over C. Europe, Italy and the W. Mediterranean. More precisely, the highest upper tropospheric tracer influence occurs to the south of the N. European anticyclone and it is progressively strengthened between 7 and 9 of May while high ozone is observed over the whole anticyclonic area. In general, over that area the observed high values of the upper tropospheric tracer indicate considerable subsidence at 5 km altitude (not shown), which becomes even stronger and more extended at the at 3 km and 1.5 km altitudes (Fig. 10). Therefore, the downward transport of upper tropospheric ozone is influencing the lower troposphere and the boundary layer over the examined location. The observed patterns, based on CHIMERE tracer simulations are quite consistent with the above described analysis based on meteorological charts and IASI satellite measurements (Figs 7, 9). Overall, there is a good agreement between the CHIMERE tracer simulations, the composite meteorological maps (Fig. 7) and the IASI satellite measurements (Figs 7, 9), showing an extended region of subsiding dry air masses over eastern and central Europe. As mentioned previously, during the afternoon hours the influence of the free troposphere on the boundary layer is maximized through vertical mixing and thus the surface ozone mixing ratios could be increased by the entrainment of subsiding ozone-rich air.

Regarding the comparison of the CHIMERE ozone field at 3 km with IASI at 700hPa there is in general a good agreement over Italy and the central Mediterranean but there are differences in E. Europe (lower CHIMERE values) and N. Europe (higher CHIMERE values), which might imply an underestimation of tropospheric transport in E. Europe or overestimation of photochemistry in N. Europe. It should be reminded that similar features appear also in the April episode, described previously. Nevertheless, as mentioned also for the April episode, it should be kept in mind that for a direct quantitative comparison between CHIMERE and IASI data, an application of IASI averaging kernels (smoothing functions) to CHIMERE output would be required (Eremenko et al., 2008).

In Figure 11 the HYSPLIT back-trajectories during the episode at EMEP stations in Italy (IT04) and France (FR10, FR14) show subsiding air masses arriving either from the north after performing a circular clockwise movement or from the NE (E. Europe and Russia) where high tropospheric ozone mixing ratios have been recorded by IASI (Figs. 7, 9). This is an additional confirmation that air masses originating from areas with high tropospheric ozone mixing ratios transport ozone down to the ground, leading to high surface ozone values.

3.3.1 Ozone vertical profiles over Payerne, Uccle and Hohenpeissenberg during the May 2008 ozone episode

Due to the more complex nature of the May 7-9, 2008 ozone episode, the vertical ozone profiles at three European ozone sounding stations (Payerne-Switzerland, Hohenpeissenberg-Germany and Uccle-Belgium) were taken into account for the analysis and the respective vertical ozone measurements for each station are shown in Fig 12.

It has to be reminded that the Payerne site is one of the two Swiss stations, where the rural afternoon surface ozone values during the May episode were about 75 ppb (Fig 1). The composite meteorological maps (Figs 7, 8) indicate that the Payerne site was within the area influenced by subsidence. As observed in Fig. 12 a layer with the tropospheric ozone maximum mixing ratio and low relative humidity is at the beginning of the event (on May 5) located between 5 and 6 km altitude. On May 7 a similar layer is seen at a somewhat lower altitude and on May 9 the tropospheric ozone maximum is found below 2000 m altitude. It has to be added that on May 12, at the end of the episode, the vertical ozone profile has changed completely and the ozone mixing ratios up to 6 km were about 60 ppb (not shown). As mentioned in the meteorological analysis of the episode (Figs 7, 8), the downward ozone transport from the ozone-rich lower troposphere to the boundary layer during the 5-9 May period with strong and persistent subsidence, is reflected clearly in the ozone profiles over Payerne (Fig. 12). Based on the observed conditions the plausible explanation is that an "ozone fumigation" of the boundary layer occurred between 5-9 May when the ozone levels increased by at least 20 ppb, following corresponding changes in the lower troposphere and indicating that this ozone event is related to downward transport of ozone from higher altitudes towards the boundary layer.

Similar observations could be made at Hohenpeissenberg and Uccle during the May 5-9 period (Fig. 12) where high ozone layers are also observed in the lower troposphere (around 80–100 ppb at 3-5 km on May 5 over both sites) and which clearly move downwards. The observed pattern is in agreement with the strong and persistent subsidence observed over the area during the examined days, as it was the case for Payerne. As shown in the vertical ozone soundings (Fig. 12) the high ozone tongue in the troposphere is going down rapidly at a 1-2 km /day rate. At the same time over the examined area the positive vertical velocity omega observed are associated with dry air (Fig. 7), indicating subsidence from the upper troposphere all the way down to the surface.

It has to be noticed at this point that vertical ozone profiles over the airports of Frankfurt and London carried out in the framework of the MOZAIC project (Marenco et al., 1998; Thouret et al., 2006) during the examined period show almost exactly the same picture (not shown).

Taking into account all the above information regarding the May episode, the following remarks regarding the tropospheric ozone distribution could be made:

a). The IASI satellite measurements shows that over N. Atlantic and to the west of the N. European anticyclone (present at all tropospheric pressure levels up to 300hPa) there are high amounts of ozone in the upper and lower troposphere.

b). The anticyclone transports these air masses from the west to the east in a clockwise rotating movement.

c). Over E. Europe and at the southern part of the anticyclone the air masses show strong signs of subsidence (downward vertical velocities, dry air), which is particularly enhanced in the vicinity of the strong low-pressure system over eastern Europe.

d). A significant ozone decrease in the upper troposphere is observed over the region covered by the N. European anticyclone followed by a slight but extended ozone increase in the lower troposphere, located over the area with intense subsidence (Central Europe) to the south of the anticyclone, with a several day time-shift.

In summarizing the observations on the May 7-9, 2008 episode an important question is to which extent the high surface ozone levels observed at first in countries surrounding the western Mediterranean basin but also over a large area in central Europe are influenced by entrainment of ozone rich air from higher layers of the troposphere. An interesting feature is that during the examined period an extended area of strong and persistent downward movement of air masses is observed over Central Europe and lasts for many days. Another important observation is that the wind makes a circular downward motion around the anticyclone while this air current is influenced from regions of very high tropospheric ozone surrounding the anticyclone (located over the observed low pressure systems), according to IASI observations. The high ozone areas coincide very well with extended areas of low humidity as observed in the 850hPa level charts but also at higher tropospheric levels. At the same time, the vertical ozone profiles over Payerne, Uccle and Hohenpeissenberg show mixing ratios at 60-80 ppb on the top of the boundary layer. It should be noticed that all the above sites are located more or less within the region of high subsidence as the meteorological analysis shows. The CHIMERE tracer simulation experiments are in very good agreement with the above observational analysis. As observed, during this episode the high measured tropospheric ozone background values contribute very significantly, through subsidence, to enhanced ozone values especially over France, Switzerland, northern Italy, and the Western Mediterranean basin, while regional ozone photochemical production is the dominant factor for ozone enhancement over the British Islands, the North Sea as well as on the Iberia peninsula and parts of France (Fig. 10, Annex Fig. XII).

Summarizing all the above, during the examined May episode as well as in the previous April episode, high atmospheric pressures prevail over the Western Mediterranean and Central Europe while low-pressure systems are observed in Eastern Europe. In general, both examined episodes (26-27 April 2008 and 7-9 May 2008) seem to show comparable characteristics: At first, very strong positive omega anomalies (strong downward air motion or subsidence) are observed over large areas including the Italian peninsula and Central Europe. At the same time, strong negative specific humidity anomalies and negative precipitable water anomalies (indicating dry air in the troposphere) are detected. An interesting feature is that the subsidence area is located at the interface of positive and negative anomalies of geopotential heights and temperature. For the May episode, although the major anticyclone seems to be located away from the Mediterranean basin to the north, a large-scale downward transport towards the Mediterranean according to the meteorological analysis is observed. It comes out from the above analysis that the interpretation of the back trajectory information is much more efficient if it is done in combination with the examination of the meteorological charts (and ideally supported by satellite measurements and modelling simulations), so that the regions with strong subsidence and dry air, are detected and taken into account in the interpretation.

3.4 Diurnal variation of surface ozone and humidity during the ozone episodes

The measurements of surface ozone, relative humidity and temperature at the EMEP site at Ispra, Italy, (Jensen, 2016) have been used during the April and May episodes in order to observe the relationship between ozone and absolute humidity (Fig. 13), which could be a good indicator for the detection of the free tropospheric influence to the boundary layer being insensitive to the diurnal temperature variation. Absolute humidity is shown in units of hPa water vapor partial pressure, calculated from the relative humidity using the August-Roche-Magnus formula to find the saturated water vapor partial pressure at the measured temperature. The ozone mixing ratios show a characteristic diurnal variation with a minimum during the night, followed by a rapid increase in the morning when the nocturnal boundary layer breaks down and air from the above layer reaches the ground. For all days with high ozone during the May episode and for some days during the April episode the ozone increase at mid-day with the maximum vertical mixing is clearly anticorrelated with absolute humidity. This is compatible with the fact that the Ispra site, according to the meteorological analysis presented above, during the whole duration of the May episode is expected to be influenced by subsidence of dry air while during the April episode much stronger anticorrelations and lower absolute humidity levels are observed for some days. Based on the presented example, a first identification of possible direct tropospheric influence to the boundary layer air could be performed at air pollution monitoring stations potentially influenced by tropospheric subsidence.

4 Conclusions

In this paper, the investigation of the regional ozone episodes in the western Mediterranean and the surrounding countries is focused on the spring season.

Based on the ozone measurements at the EMEP rural ozone stations surrounding the western Mediterranean basin (as well as the EEA-AirBase network), it is observed that episodic periods of high ozone may last for several days and they can be detected at several countries at the same time.

An interesting result was that the examined ozone episodes are linked to meteorological conditions very similar to those observed in the eastern Mediterranean (Kalabokas et al., 2013; Doche at al., 2014; Kalabokas et al., 2015), related essentially with transport of ozone-rich tropospheric air masses and the atmospheric subsidence phenomenon. Based on the analysis of the selected springtime ozone episodes, the characteristics associated with high ozone mixing ratios close to the surface through important subsidence and in connection with high tropospheric ozone levels occurring in the wider area, are the following:

The geographic areas with observed deep tropospheric subsidence seem to be the transition regions between a high pressure system, located in the west sector, and a low pressure system located in the east sector, as shown in the corresponding charts of the geopotential heights. Over these areas, strong gradients of geopotential height and temperature are observed together with high omega vertical velocity values and low specific humidity values at the 850hPa as well as at higher tropospheric pressure levels. In addition, over the areas of deep tropospheric subsidence, negative temperature anomalies are observed at these levels and also high vector wind speeds, which means that subsidence is associated with strong advection. The above observational analysis is in very good agreement with IASI satellite measurements and CHIMERE tracer simulation experiments.

The present approach, using meteorological charts, IASI tropospheric ozone satellite measurements, CHIMERE tracer simulations and back trajectories for the analysis of selected spring ozone episodes, shows to be quite efficient in the analysis of atmospheric conditions and transport patterns associated with the episodes, which need to be adequately described in numerical chemical-transport models used for simulations of air pollution. It can be useful for the study of the tropospheric influence on the boundary layer and the ground surface, especially for tracing large scale deep subsidence events (downward movements of generally dry air masses) when analyzing surface (and vertical, if available) measurements at sites in the Mediterranean basin, where this phenomenon is quite frequent, and also in other places worldwide. For example, similar field observations on the influence of upper atmospheric layers on the boundary layer and surface measurements have been reported at some locations in the United States (Parrish et al., 2010; Cooper et al., 2011; Langford et al., 2015). In addition, the consideration for the analysis of ozone measurements presented above is in agreement with recent observations in Atlantic and European regions indicating significant tropospheric (and even stratospheric) influence to the surface and boundary layer ozone measurements (Trickl et al., 2010; Trickl et al., 2011; Logan et al., 2012; Cuevas et al., 2013; Hess and Zbinden, 2013; Cooper et al., 2014; Parrish et al., 2014).

Regarding the environmental policy issues, it has to be underlined that for ozone, which is a pollutant regulated by the EU, it appears that there are some time periods during the warm period of the year, lasting for several days, when the free troposphere influences significantly the boundary layer to such extent that the air quality standards might be exceeded. This phenomenon seems to be associated with an important impact of photochemical ozone production following primary air pollutant emission at larger geographical scales, including transport of air pollutants on a hemispheric scale from e.g. the US and China. The origin of the atmospheric ozone entering the boundary layer might be upper tropospheric or stratospheric but it could also be from the lower or the middle troposphere during stagnant regional conditions when photochemical ozone is produced over the continent.

Further detailed and quantitative studies of this phenomenon appear to be needed to improve our understanding of the mechanisms associated with intercontinental pollution as well as regional photochemical pollution could be improved, already highlighted by the work of the HTAP (Hemispheric Transport of Air Pollution) project. The Mediterranean region which seems to be mostly affected is the Eastern Mediterranean, where the 60 ppb EU standard is very frequently exceeded during the warm period of the year and especially during July-August when the atmospheric subsidence is a quite common atmospheric feature and almost quasi-permanent, but as shown in the present study, also in the Western Mediterranean a similar mechanism could be observed, especially during the spring season. The strategies for obtaining compliance with the EU ozone standard may need to be reconsidered by taking into account the contribution from regional and intercontinental transport.

Acknowledgements

Acknowledgement is made for the use of ECMWF's computing and archive facilities in this research. Acknowledgement is also made for the composite weather maps were provided by the NOAA/ESRL Physical Sciences Division, Boulder Colorado from their Web site at http://www.cdc.noaa.gov/. The authors also acknowledge the NOAA Air Resources Laboratory (ARL) for the provision of the HYSPLIT transport and

dispersion model and/or READY website (http://www.ready.noaa.gov) used in this publication. Also, Dr. A. Volz-Thomas, FZ-Juelich, is acknowledged for interesting discussion as well as Dr. C. Repapis, Academy of Athens, for useful comments on the manuscript. JRC is acknowledged for an EU grant (cat. 40) to one of the authors (P. K.). Our particular thanks go to the operators of the following air quality monitoring stations: Cabo de Creus in Spain, Morvan and Montandon in France, Payerne and Chaumont in Switzerland, Montelibretti and Ispra in Italy and Giordan Lighthouse in Malta. This work was performed using HPC resources from GENCI-TGCC (Grant 2016-[t20155017232]).

References

Beekmann, M. and Vautard R. (2010), A modelling study of photochemical regimes over Europe: robustness and variability, Atmos. Chem. Phys., 10, 10067-10084.

Beekmann, M., Ancellet, G. and Megie, G. 1994. Climatology of tropospheric ozone in southern Europe and its relation to potential vorticity, J. Geoph. Res., 99, 12841-12853.

Bonasoni, P., Stohl, A., Cristofanelli, P., Calzolari, F., Colombo, T. and Evangelisti, F. 2000. Background ozone variations at Mt. Cimone station. Atmos. Environ. 34, 5183-5189.

Boynard, A., Clerbaux, C., Coheur, P.-F., Hurtmans, D., Turquety, S., George, M., Hadji-Lazaro, J., Keim, C., and Meyer-Arnek, J. 2009. Measurements of total and tropospheric ozone from IASI: comparison with correlative satellite, ground-based and ozonesonde observations, Atmos. Chem. Phys., 9, 6255–6271, doi:10.5194/acp-9-6255-2009.

Clarisse, L., R'Honi, Y., Coheur, P.-F., Hurtmans, D., and Clerbaux, C., 2011. Thermal infrared nadir observations of 24 atmospheric gases, Geophys. Res. Lett., 38, L10802, doi:10.1029/2011GL047271.

Clerbaux, C., Boynard, A., Clarisse, L., George, M., Hadji-Lazaro, J., Herbin, H., Hurtmans, D., Pommier, M., Razavi, A., Turquety, S., Wespes, C., and Coheur, P.-F. 2009. Monitoring of atmospheric composition using the thermal infrared IASI/MetOp sounder, Atmos. Chem. Phys., 9, 6041–6054, doi:10.5194/acp-9-6041-2009.

Coheur, P.-F., Barret, B., Turquety, S., Hurtmans, D., Hadji-Lazaro, J., and Clerbaux, C. 2005. Retrieval and characterization of ozone vertical profiles from a thermal infrared nadir sounder, J. Geophys. Res., 110, D24303, doi:10.1029/2005JD005845.

Cooper, O.R., Oltmans, S.J., Johnson, B.J., Brioude, J., Angevine, W., Trainer, M., Parrish, D. D., Ryerson, T. R., Pollack, I., Cullis, P. D., Ives, M.,A., Tarasick D.W., Al-Saadi, J., Stajner, I. 2011. Measurement of western U.S. baseline ozone from the surface to the tropopause and assessment of downwind impact regions. J. Geophys. Res 116:D00V03. doi:10.1029/2011JD016095

Cooper, O. R., Gao, R.-S., Tarasick, D., Leblanc, T., Sweeney, C. 2012. Long-term ozone trends at rural ozone monitoring sites across the United States, 1990–2010. J. Geophys. Res 117: D22307. doi:10.1029/2012JD018261

Cooper, O. R., Parrish, D. D., Ziemke, J., Balashov, N. V., Cupeiro, M., Galbally, I. E., Gilge, S., Horowitz, L., Jensen, N. R., Lamarque, J.-F., Naik, V., Oltmans, S. J., Schwab, J., Shindell, D. T., Thompson, A. M., Thouret, V., Wang, Y., Zbinden, R. M. 2014. Global distribution and trends of tropospheric ozone: An observation-based review. Elementa: Sci. of the Anthropocene. 2: 000029, doi: 10.12952/journal.elementa.000029

Coman, A., Foret, G., Beekmann, M., Eremenko, M., Dufour, G., Gaubert, B., Ung, A., Schmechtig, C., Flaud, J.-M., and Bergametti, G. 2012. Assimilation of IASI partial tropospheric columns with an Ensemble Kalman Filter over Europe, Atmos. Chem. Phys., 12, 2513–2532, doi:10.5194/acp-12-2513-2012.

Cristofanelli, P., Scheel, H.-E., Steinbacher, M., Saliba, M., Azzopardi, F., Ellul, R., Froehlich, M., Tositti, L., Brattich, E., Maione, M., Calzolari, F., Duchi, R., Landi, T.C., Marinoni, A. and Bonasoni P. 2015. Long-term surface ozone variability at Mt. Cimone WMO/GAW global station (2165 m a.s.l., Italy). Atmos. Environ. 101, 23-33.

Cuevas, E., González, Y., Rodríguez, S., Guerra, J.C., Gómez-Peláez, A.J., Alonso Pérez, S., Bustos, J., Milford, C. 2013. Assessment of atmospheric processes driving ozone variations in the subtropical North Atlantic free troposphere, Atmos. Chem. Phys 13:1973–1998.

Delmas, R., Mégie, G., and Peuch, V.-H. 2005. Physique et chimie de l'atmosphère, Ed. Belin, Coll. Echelles, 640

Doche, C., Dufour, G., Foret, G., Eremenko, M., Cuesta, J., Beekmann, M., and Kalabokas, P. 2014. Summertime tropospheric-ozone variability over the Mediterranean basin observed with IASI, Atmos. Chem. Phys., 14, 10589–10600.

Draxler, R.R. and Rolph, G.D. 2015. HYSPLIT (HYbrid Single-Particle Lagrangian Integrated Trajectory) Model access via NOAA ARL READY Website (http://www.arl.noaa.gov/HYSPLIT.php). NOAA Air Resources Laboratory, College Park, MD.

EEA, 2015: http://www.eea.europa.eu/themes/air/air-quality/map/airbase

EMEP, 2015. EMEP, Chemical Coordinated Center, www.emep.int

Dufour, G., Eremenko, M., Orphal, J., and Flaud, J.-M. 2010. IASI observations of seasonal and day-to-day variations of tropospheric ozone over three highly populated areas of China: Beijing, Shanghai, and Hong Kong, Atmos. Chem. Phys., 10, 3787–3801, doi:10.5194/acp-10-3787-2010.

Dufour, G., Eremenko, M., Griesfeller, A., Barret, B., LeFlochmoën, E., Clerbaux, C., Hadji-Lazaro, J., Coheur, P.-F. and Hurtmans D., Validation of three scientific ozone products retrieved from IASI spectra using ozonesondes, Atmos. Meas. Tech., 5, 611-630, 2012.

Dufour, G., Eremenko, M., Cuesta, J., Doche, C., Foret, G., Beekmann, M., Cheiney, A., Wang, Y., Cai, Z., Liu, Y., Takigawa, M., Kanaya, Y., and Flaud, J.-M.: Springtime daily variations in lower-tropospheric ozone over east Asia: the role of cyclonic activity and pollution as observed from space with IASI, Atmos. Chem. Phys., 15, 10839-10856, doi:10.5194/acp-15-10839-2015, 2015.

Eremenko, M., Dufour, G., Foret, G., Keim, C., Orphal, J., Beekmann, M., Bergametti, G., and Flaud, J.-M. 2008. Tropospheric ozone distributions over Europe during the heat wave in July 2007 observed from infrared nadir spectra recorded by IASI, Geophys. Res. Lett., 35, L18805, doi:10.1029/2008GL034803.

Fishman, J., Wozniak, A. E., and Creilson, J. K. 2003. Global distribution of tropospheric ozone from satellite measurements using the empirically corrected tropospheric ozone residual technique: Identification of the regional aspects of air pollution, Atmos. Chem. Phys., 3, 893–907, doi:10.5194/acp-3-893-2003.

Foret, G., Hamaoui, L., Schmechtig, C., Eremenko, M., Keim, C., Dufour, G., Boynard, A., Coman, A., Ung, A., and Beekmann, M. 2009. Evaluating the potential of IASI ozone observations to constrain simulated surface ozone concentrations, Atmos. Chem. Phys., 9, 8479–8491, doi:10.5194/acp-9-8479-2009.

Fuhrer, J. 2009. Ozone risk for crops and pastures in present and future climates, Naturwissenschaften, 96, 173–194.

Hess, P.G., Zbinden, R., 2013. Stratospheric impact on tropospheric ozone variability and trends: 1990–2009, Atmos. Chem. Phys., 13, 649–674.

George, M., Clerbaux, C., Hurtmans, D., Turquety, S., Coheur, P.-F., Pommier, M., Hadji-Lazaro, J., Edwards, D. P., Worden, H., Luo, M., Rinsland, C., and McMillan,W. 2009. Carbon monoxide distributions from the IASI/METOP mission: evaluation with other space-borne remote sensors, Atmos. Chem. Phys., 9, 8317–8330, doi:10.5194/acp-9-8317-2009.

Gerasopoulos, E., Kouvarakis, G., Vrekoussis, M., Kanakidou, M., Mihalopoulos, N., 2005. Ozone variability in the marine boundary layer of the Eastern Mediterranean based on 7-year

Observations, J. Geoph. Res., 110, D15309.

Guenther, A., Karl, T., Harley, P., Wiedinmyer, C., Palmer, P. I., and Geron. C. 2006. Estimates of global terrestrial isoprene emissions using MEGAN (Model of Emissions of Gases and Aerosols from Nature). Atmos. Chem. Phys., 6, 3181–3210, www.atmos-chem-phys.net/6/3181/2006/

HTAP report, 2010. Hemispheric Transport of Air Pollution 2010. Part A: Ozone and Particulate Matter, Air Pollution Studies No 17, United Nations Econimic Commission for Europe, ISBN 978-92-1-117043-6

IPCC: Climate Change 2007: The Physical Science Basis, Contribution of Working Group I to the Fourth Assessment Report of the Intergovernmental Panel on Climate Change, edited by: Solomon, S., Qin, D., Manning, M., Chen, Z., Marquis, M., Averyt, K. B., Tignor, M., and Miller, H. L., Cambridge University Press, Cambridge, United Kingdom and New York, NY, USA, 2007.

Johnson, J. E., Sundet, J. K., and Tarrason, L. 2001. Model calculations of present and future levels of ozone and ozone precursors with a global and regional model, Atmos. Environ., 35, 525–537.

Jensen, N.R. (2016), personal communication.

Kalabokas, P. D., Viras, L. G., Bartzis, J. G., and Repapis, C. C. 2000. Mediterranean rural ozone characteristics around the urban area of Athens, Atmosph. Environ., 34, 5199–5208.

Kalabokas, P. D. and Repapis, C. C. 2004. A climatological study of rural surface ozone in central Greece, Atmos. Chem. Phys., 4, 1139–1147, doi:10.5194/acp-4-1139-2004.

Kalabokas, P. D., Volz-Thomas, A., Brioude, J., Thouret, V., Cammas, J.-P., and Repapis, C. C. 2007. Vertical ozone measurements in the troposphere over the Eastern Mediterranean and comparison with Central Europe, Atmos. Chem. Phys., 7, 3783–3790, doi:10.5194/acp-7-3783-2007.

Kalabokas, P. D., Mihalopoulos, N., Ellul, R., Kleanthous, S., and Repapis, C. C. 2008. An investigation of the meteorological and photochemical factors influencing the background rural and marine surface ozone levels in the Central and Eastern Mediterranean, Atmos. Environ., 42, 7894–7906

Kalabokas, P. D., Cammas, J.-P., Thouret, V., Volz-Thomas, A., Boulanger, D., and Repapis, C. C. 2013. Examination of the atmospheric conditions associated with high and low summer ozone levels in the lower troposphere over the eastern Mediterranean, Atmos. Chem. Phys., 13, 10339–10352, doi:10.5194/acp-13-10339-2013.

Kalabokas, P. D., Thouret, V., Cammas, J.-P., Volz-Thomas, A., Boulanger, D., and Repapis, C. C. 2015. The geographical distribution of meteorological parameters associated with high and low summer ozone levels in the lower troposphere and the boundary layer over the Eastern Mediterranean (Cairo case). Tellus B, 67, 27853, http://dx.doi.org/10.3402/tellusb.v67.27853

Kalnay, E., Kanamitsu, M., Kistler, R., Collins, W., Deaven, D., Gandin, L., Iredell, M., Saha, S., White, G., Woolen, J., Zhu, Y., Chelliah, M., Ebisuzaki, W., Higgins, W., Janowiak, J., Mo, K. C., Ropelewski, C., Wang, J., Leetmaa, A., Reynolds, R., Jenne, R., and Joseph, D. 1996. The NCEP/NCAR Reanalysis 40-year Project, B. Am. Meteorol. Soc., 77, 437–471.

Kleanthous, S., Vrekoussis, M., Mihalopoulos, N., Kalabokas, P. and Lelieveld, J. 2014. On the temporal and spatial variation of ozone in Cyprus. Sc. of the Tot. Environ. 476–477 (2014), 677–687.

Kourtidis, K., Zerefos, C., Rapsomanikis, S., Simeonov, V., Balis, D., Perros, P. E., Thomson, A. M., Witte, J., Calpini, B., Sharobiem, W. M., Papayiannis, A., Mihalopoulos, N., and Drakou, R. 2002. Regional levels of ozone in the troposphere over eastern Mediterranean, J. Geophys. Res., 107, 8140, doi:10.1029/2000JD000140.

Kouvarakis, G., Vrekoussis, M., Mihalopoulos, N., Kourtidis, K., Rappenglueck, B., Gerasopoulos, E., and Zerefos, C. 2002. Spatial and temporal variability of tropospheric ozone in the boundary layer above the Aegean Sea (eastern Mediterranean), J. Geophys. Res., 107, 8137, doi:10.1029/2000JD000081.

Kuenen, J. J. P., Visschedijk, A. J. H., Jozwicka, M. and Denier van der Gon, H. A. C. 2014. TNO-MACC_II emission inventory; a multi-year (2003–2009) consistent high-resolution European emission inventory for air quality modeling, Atmos. Chem. Phys., 14, 10963-10976, doi:10.5194/acp-14-10963-2014, 2014.

Langford, A.O., Sen, C.J., Alvarez, R.J., Brioude, J., Cooper, O.R., Holloway, J.S., Lind, M.Y., Marchbanksa, R.D., Pierce, R.B., Sandberg, S.P., Weickmann, A.M., Williams, E.J. 2015. An Overview of the 2013 Las Vegas Ozone Study (LVOS): Impact of stratospheric intrusions and long-range transport on surface air quality. Atmos. Environ., 109, 305–322.

1 Levy, J. I., Carrothers, T. J., Tuomisto, J. T., Hammitt, J. K., and Evans, J. S. 2001. Assessing the Public Health
2 Benefits of Reduced Ozone Concentrations, Environ. Health Perspect., 109, 1215– 1226.

3 Lelieveld, J., Berresheim, H., Borrmann, S., Crutzen, P. J., Dentener, F. J., Fischer, H., Feichter, J., Flatau, P. J.,
4 Heland, J., Holzinger, R., Korrmann, R., Lawrence, M. G., Levin, Z., Markowicz, K. M., Mihalopoulos, N.,
5 Minikin, A., Ramanathan, V., de Reus, M., Roelofs, G. J., Scheeren, H. A., Sciare, J., Schlager, H., Schultz, M.,
6 Siegmund, P., Steil, B., Stephanou, E. G., Stier, P., Traub, M., Warneke, C., Williams, J., and Ziereis, H. 2002.
7 Global air pollution crossroads over the Mediterranean, Science, 298, 794–799.

8 Lelieveld, J. 2009. Air pollution and climate, in: The Physical Geography of the Mediterranean, edited by:
9 Woodward, J. C., Oxford University Press, 599–614.

10 Li, Q., Jacob, D. J., Logan, J. A., Bey, I., Yantosca, R. M., Liu, H., Martin, R. V., Fiore, A. M., Field, B. D.,
11 Duncan, B. N., and Thouret, V. 2001. A tropospheric ozone maximum over the Middle East, Geophys. Res.
12 Lett., 28, 3235–3238, doi:10.1029/2001GL013134.

13 Liu, X., Chance, K. V., Sioris, C. E., Spurr, R. J. D., Kurosu, T. P., Martin, R. V., and Newchurch, M. J. 2005.
14 Ozone profile and tropospheric ozone retrievals from Global Ozone Monitoring Experiment: Algorithm
15 description and validation, J. Geophys. Res., 110, D20307, doi:10.1029/2005JD006240.

16 Liu, J. J., Jones, D. B. A., Worden, J. R., Noone, D., Parrington, M., and Kar, J. 2009. Analysis of the
17 summertime build-up of tropospheric ozone abundances over the Middle East and North Africa as observed by
18 the Tropospheric Emission Spectrometer instrument, J. Geophys. Res., 114, D05304,
19 doi:10.1029/2008JD010993.

20 Logan, J. A., Staehelin, J., Megretskaia, I. A., Cammas, J.-P., Thouret, V., Claude, H., De Backer, H.,
21 Steinbacher, M., Scheel, H.-E., Stübi, R., Fröhlich M. and Derwent R. 2012. Changes in ozone over Europe:
22 Analysis of ozone measurements from sondes, regular aircraft (MOZAIC) and alpine surface sites, J. Geophys.
23 Res., 117, D09301, doi:10.1029/2011JD016952.

24 Marenco, A., Thouret, V., Nédélec, P., Smit, H., Helten, M., Kley, D,. Karcher, F., Simon, P., Law, K., Pyle, J.,
25 Poschmann, G., Von Wrede, R., Hume, C., and Cook, T. 1998. Measurements of ozone and water vapor by
26 Airbus in-service aircraft: The MOZAIC airborne program. An overview, J. Geophys. Res., 103, 25631–25642.

27 Menut, L., Bessagnet, B., Khvorostyanov, D., Beekmann, M., Blond, N., Colette, A., Coll, I., Curci, G., Foret,
28 G., Hodzic, A., Mailler, S., Meleux, F., Monge, J.-L., Pison, I., Siour, G., Turquety, S., Valari, M., Vautard, R.,
29 and Vivanco, M. G. 2013. CHIMERE 2013: a model for regional atmospheric composition modelling, Geosci.
30 Model Dev., 6, 981–1028, doi:10.5194/gmd-6-981-2013.

31 Millán, M. M., Salvador, R., Mantilla, E., and Kallos, G. 1997. Photo-oxidant dynamics in the western
32 Mediterranean in summer: Results from European research projects, J. Geoph. Res. 102: 8811–23.

33 Millan, M.M., Mantilla, E., Salvador, R., Carratalá, R., Sanz, M. J., Alonso, L., Gangioti, G., and Navazo, M.
34 2000. Ozone cycles in the western Mediterranean basin: Interpretation of monitoring data in complex coastal
35 terrain. J. Appl. Meteor. 39, 487– 508.

Monks, P. S., 2000. A review of the observations and origins of the spring ozone maximum, Atmos. Environ., 34, 3545–3561.

Monks, P. S., Archibald, A. T., Colette, A., Cooper, O., Coyle, M., Derwent, R., Fowler, D., Granier, C., Law, K. S., Mills, G. E., Stevenson, D. S., Tarasova, O., Thouret, V., von Schneidemesser E., Sommariva, R., Wild, O., and Williams, M. L. 2015. Tropospheric ozone and its precursors from the urban to the global scale from air quality to short-lived climate forcer, Atmos. Chem. and Phys., 15, 8889-8973.

Nolle, M., Ellul, R., Heinrich, G., and Güsten, H. 2002. A longterm study of background ozone concentrations in the central Mediterranean—diurnal and seasonal variations on the island of Gozo, Atmospheric Environment 36: 1391–402.

Paoletti, E. 2006. Impact of ozone on Mediterranean forests: A Review, Environ. Pollut., 144, 463–474.

Parrish, D. D., Aikin, K. C., Oltmans, S. J., Johnson, B. J., Ives, M., and Sweeny, C. 2010. Impact of transported background ozone inflow on summertime air quality in a California ozone exceedance area, Atmos. Chem. Phys., 10, 10093–10109, doi:10.5194/acp-10-10093-2010.

Parrish, D.D., Law, K.S., Staehelin, J., Derwent, R., Cooper, O.R., Tanimoto, H., Volz-Thomas, A., Gilge, S., Scheel, H.-E., Steinbacher, M., and Chan, E. 2013. Lower tropospheric ozone at northern mid-latitudes: Changing seasonal cycle. Geophys. Res. Lett 40: 1631–1636. doi:10.1002/grl.50303.

Parrish, D. D., Lamarque, J.-F., Naik, V., Horowitz, L., Shindell, D. T., Staehelin, J., Derwent, R., Cooper, O. R., Tanimoto, H., Volz-Thomas, A., Gilge, S., Scheel, H.-E., Steinbacher, M., and Fröhlich, M. 2014. Long-term changes in lower tropospheric baseline ozone concentrations: Comparing chemistry-climate models and observations at northern midlatitudes, J. Geophys. Res. Atmos., 119, 5719–5736, doi:10.1002/ 2013JD021435.

Querol X., Alastuey A., Orio A., Pallares M., Reina F., Dieguez JJ., Mantilla E., Escudero M., Alonso L., Gangoiti G., Millán M. 2016. On the origin of the highest ozone episodes in Spain. Science of the Total Environment, 572, 379-389.

Richards, N. A. D., Arnold, S. R., Chipperfield, M. P., Miles, G., Rap, A., Siddans, R., Monks, S. A., and Hollaway, M. J. 2013. The Mediterranean summertime ozone maximum: global emission sensitivities and radiative impacts, Atmos. Chem. Phys., 13, 2331–2345, doi:10.5194/acp-13-2331-2013.

Rodwell, M. J. and Hoskins, B. J. 1996. Monsoons and the dynamics of deserts, Q. J. R. Meteorol. Soc., 122, 1385–1404, doi:10.1002/qj.49712253408.

Rodwell, M. J. and Hoskins, B. J. 2001. Subtropical anticyclones and summer monsoons, J. Climate, 14, 3192–3211.

Rouil L., C.Honore, R.Vautard, M.Beekmann, B.Bessagnet, L.Malherbe, F.Meleux, A.Dufour, C.Elichegaray, J-M.Flaud, L.Menut, D.Martin, A.Peuch, V-H.Peuch, N.Poisson, 2009, PREV'AIR : an operational forecasting and mapping system for air quality in Europe, BAMS, DOI: 10.1175/2008BAMS2390.1

Safieddine, S., Boynard, A., Coheur, P.-F., Hurtmans, D., Pfister, G., Quennehen, B., Thomas, J. L., Raut, J.-C., Law, K. S., Klimont, Z., Hadji-Lazaro, J., George, M., and Clerbaux C. 2014. Summertime tropospheric ozone

assessment over the Mediterranean region using the thermal infrared IASI/MetOp sounder and the WRF-Chem model, Atmos. Chem. Phys., 14, 10119–10131, doi:10.5194/acp-14-10119-2014.

Sánchez, M. L., García, M. A., Pérez, I. A., and de Torre, B. 2008. Evaluation of surface ozone measurements during 2000–2005 at a rural area in the upper Spanish plateau, J. Atmos. Chem., 60, 137–152.

Schürmann, G. J., Algieri, A., Hedgecock, I. M., Manna, G., Pirrone, N., and Sprovieri, F. 2009. Modeling local and synoptic scale influences on ozone concentrations in a topographically complex region of Southern Italy, Atmos. Environ., 43, 4424–4434.

Seinfeld, J. H., Pandis, S. N., 2006. Atmospheric Chemistry and Physics: From Air Pollution to Climate Change, 2nd Edition, Wiley.

Sicard, P., De Marco, A., Troussier, F., Renou, C., Vas, N., Paoletti, E. 2013. Decrease in surface ozone concentrations at Mediterranean remote sites and increase in the cities. Atmos. Environ 79: 705–715.

Stohl, A., Eckhardt, S., Forster, C., James, P., and Spichtinger, N. 2002. On the pathways and timescales of intercontinental air pollution transport, J. of Geoph. Res(Atm.), 107(D23): 4684-4700.

Thouret, V., Cammas, J.-P., Sauvage, B., Athier, G., Zbinden, R., Nédélec, P., Simon, P., and Karcher, F. 2006. Tropopause referenced ozone climatology and inter-annual variability (1994–2003) from the MOZAIC programme, Atmos. Chem. Phys., 6, 1033–1051, doi:10.5194/acp-6-1033-2006.

Trickl, T., Feldmann, H., Kanter, H.-J., Scheel, H.-E., Sprenger, M., Stohl, A., and Wernli, H., 2010. Forecasted deep stratospheric intrusions over Central Europe: case studies and climatologies, Atmos. Chem. Phys., 10, 499–524, doi:10.5194/acp-10-499-2010.

Trickl, T., Bärtsch-Ritter, N., Eisele, H., Furger, M., Mücke, R., Sprenger, M., and Stohl, A. 2011. High-ozone layers in the middle and upper troposphere above Central Europe: potential import from the stratosphere along the subtropical jet stream, Atmos. Chem. Phys., 11, 9343–9366, doi:10.5194/acp-11-9343-2011.

Tyrlis, E., Lelieveld, J., and Steil, B. 2013. The summer circulation in the eastern Mediterranean and the Middle East: influence of the South Asian Monsoon, Clim. Dynam., 40, 1103–1123, doi:10.1007/s00382-012-1528-4.

Tyrlis, E., Škerlak, B., Sprenger, M., Wernli, H., Zittis, G., and Lelieveld, J., 2014. On the linkage between the Asian summer monsoon and tropopause fold activity over the eastern Mediterranean and the Middle East, J. Geophys. Res. Atmos., 119, 3202–3221, doi:10.1002/2013JD021113.

Velchev, K., Cavalli, F., Hjorth, J., Marmer, E., Vignati, E., Dentener, F., and Raes, F., 2011. Ozone over the Western Mediterranean Sea – results from two years of shipborne measurements, Atmos. Chem. Phys., 11, 675–688, doi:10.5194/acp-11-675-2011.

Worden, H. M., Logan, J. A., Worden, J. R., Beer, R., Bowman, K., Clough, S. A., Eldering, A., Fisher, B. M., Gunson, M. R., Herman, R. L., Kulawik, S. S., Lampel, M. C., Luo, M., Megretskaia, I. A., Osterman, G. B., and Shephard, M.W. 2007. Comparisons of Tropospheric Emission Spectrometer (TES) ozone profiles to ozonesondes: Methods and initial results, J. Geophys. Res., 112, D03309, doi:10.1029/2006JD007258.

WOUDC, 2015: http://woudc.org/data/explore.php

1   Zanis, P., Hadjinicolaou, P., Pozzer, A., Tyrlis, E., Dafka, S., Mihalopoulos, N., and Lelieveld, J. 2014.

2   Summertime free-tropospheric ozone pool over the eastern Mediterranean/Middle East, Atmos. Chem. Phys., 14,

3   115–132, doi:10.5194/acp-14-115-2014.

FIGURE CAPTIONS

Figure 1: (Upper panel): Day-to-day variation of the 12:00 - 18:00 afternoon ozone (in ppb) on the EMEP stations surrounding the Western Mediterranean basin for spring 2008: Spain (ES10, light blue), France (FR10-14, black), Switzerland (CH02-04, green), Italy (IT01-04, red), Malta (MT01, blue).

(Lower panel): Day-to-day variation of the 12:00 - 18:00 afternoon ozone (in ppb) on the EMEP stations close to the Western Mediterranean basin and around the Alpine region for spring 2008: France (FR10-14, black), Switzerland (CH02-04, green), Italy (IT04-JRC, red).

Figure 2: Composite NOAA/ESRL weather maps of geopotential height (upper panel-left, in m), specific humidity anomaly (upper panel-right, in Kg/Kg), vector wind (middle panel-left, in m/s), air temperature anomaly (middle panel-right, in K), omega vertical velocity (lower panel-left, in Pa/s) and IASI satellite ozone mixing ratios at 3km (lower panel-right, in ppb) for the high ozone episode of 26-27 April 2008.

Figure 3: Composite ECMWF meteorological charts of geopotential height (upper panel, in m), wind speed (middle panel, in m/s) and   vertical velocity (lower panel, in Pa/s) at 900hPa (left) and 800 hPa (right) for the high ozone episode of 26-27 April 2008.

Figure 4: Daily IASI satellite ozone measurements (ppb) at 10 km level (upper panel, in ppb) and at 3km level (middle panel, in ppb) for April 26, 2008 (left column) and April 27, 2008 (right column). Values outside the scale range are set up to the upper and lower color code respectively.

(Lower panel): Hourly average surface ozone (EEA-AirBase) mixing ratios (ppb) at 15:00 h for April 26, 2008 (left column) and for April 27, 2008 (right column). Ozone data are from the EEA-AirBase database.

Figure 5 (Upper panel): CHIMERE simulations of the ozone field at 3 km altitude (in ppb) with the iso-contours of the high tropospheric tracer (in black, arbitrary units) for April 26, 2008 (left column) and for April 27, 2008 (right column). (Lower panel): Same as in upper panel but for 1.5 km altitude.

Figure 6: Backward trajectories during the April 25-27 episode ending at EMEP rural ozone stations in Italy (IT04, upper and middle panels) and Malta (MT01, lower panel).

Figure 7: Composite NOAA/ESRL weather maps of geopotential height (upper panel-left, in m), specific humidity anomaly (upper panel-right, in Kg/Kg), vector wind (middle panel- left, in m/s) air temperature anomaly (middle panel- right, in K), omega vertical velocity (lower panel-left, in Pa/s) and IASI satellite ozone measurements at 3km (lower panel-right, in ppb) for the high ozone episode of 7-9 May 2008.

Figure 8: Composite ECMWF meteorological charts of geopotential height (upper panel, in m), wind speed (middle panel, in m/s) and vertical velocity (lower panel, in Pa/s) at 900hPa (left) and 800 hPa (right) for the high ozone episode of 7-9 May 2008.

Figure 9: Daily IASI satellite ozone measurements at 10 km level (upper panel, in ppb) and at 3km level (middle panel, in ppb) for May 7, 2008 (left column) and May 9, 2008 (right column). Values outside the scale range are set up to the upper and lower color code respectively.

(Lower panel): Hourly average surface ozone (EEA-AirBase) mixing ratios (ppb) at 15:00 h for May 7, 2008 (left column) and May 9, 2008 (right column). Ozone data are from the EEA-AirBase database.

Figure 10 (Upper panel): CHIMERE simulations of the ozone field at 3 km altitude (in ppb) with the iso-contours of the high tropospheric tracer (in black, arbitrary units) for May 7, 2008 (left column), and May 9, 2008 (right column). (Lower panel): Same as in upper panel but for 1.5 km altitude.

Figure 11: Backward trajectories during the 6-9 May 2008 ozone episode ending at EMEP rural ozone stations in Switzerland and Italy (left column) and France (right column).

Figure 12: Vertical profiles of ozone (red, ppb) and relative humidity (blue, %) over Payerne, Switzerland (left column), Hohenpeissenberg, Germany (middle column) and Uccle, Belgium (right column) on May 7, 2008 (upper panel), May 8, 2008 (middle panel) and May 9, 2008 (lower panel).

Figure 13: (Upper panel): Ozone mixing ratio (red, ppb) and absolute humidity (blue, hPa) measurements at the JRC-Ispra station during the 26-27 April 2008 ozone episode.

(Lower panel): Ozone mixing ratio (red, ppb) and absolute humidity (blue, hPa) measurements at the JRC-Ispra station during the May 7-9, 2008 ozone episode.
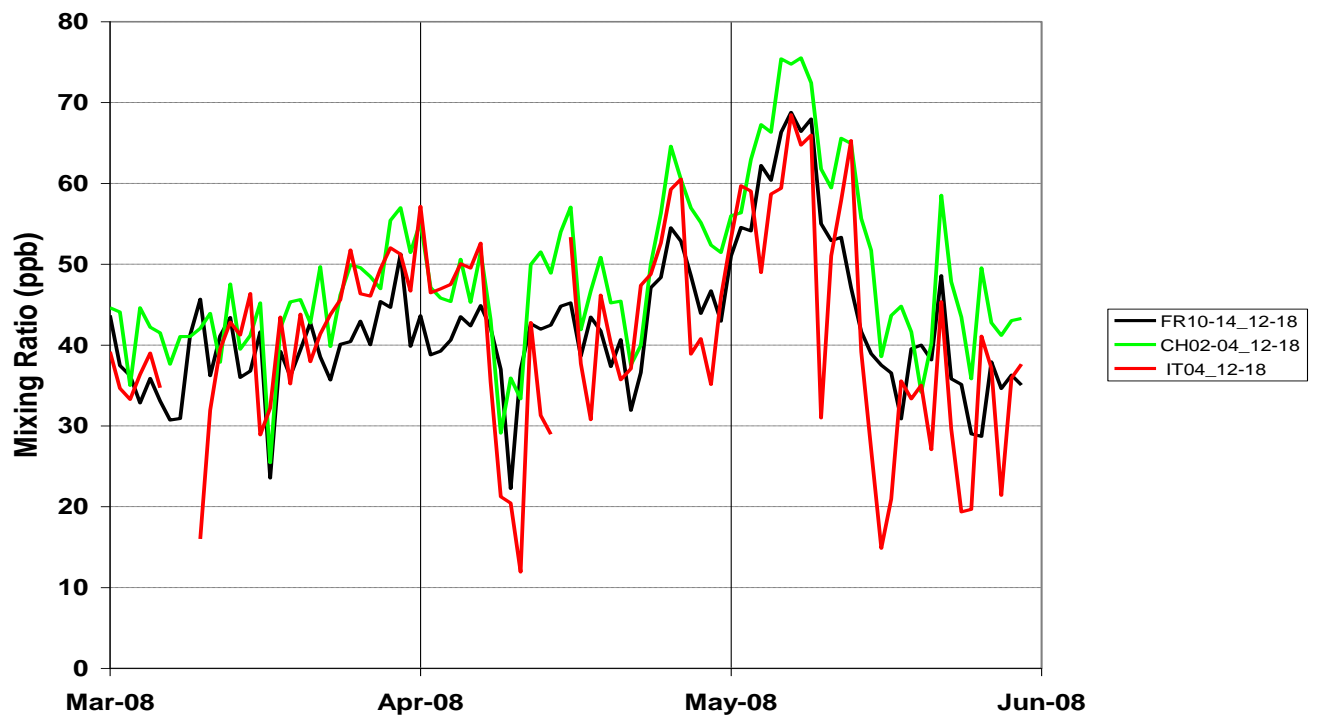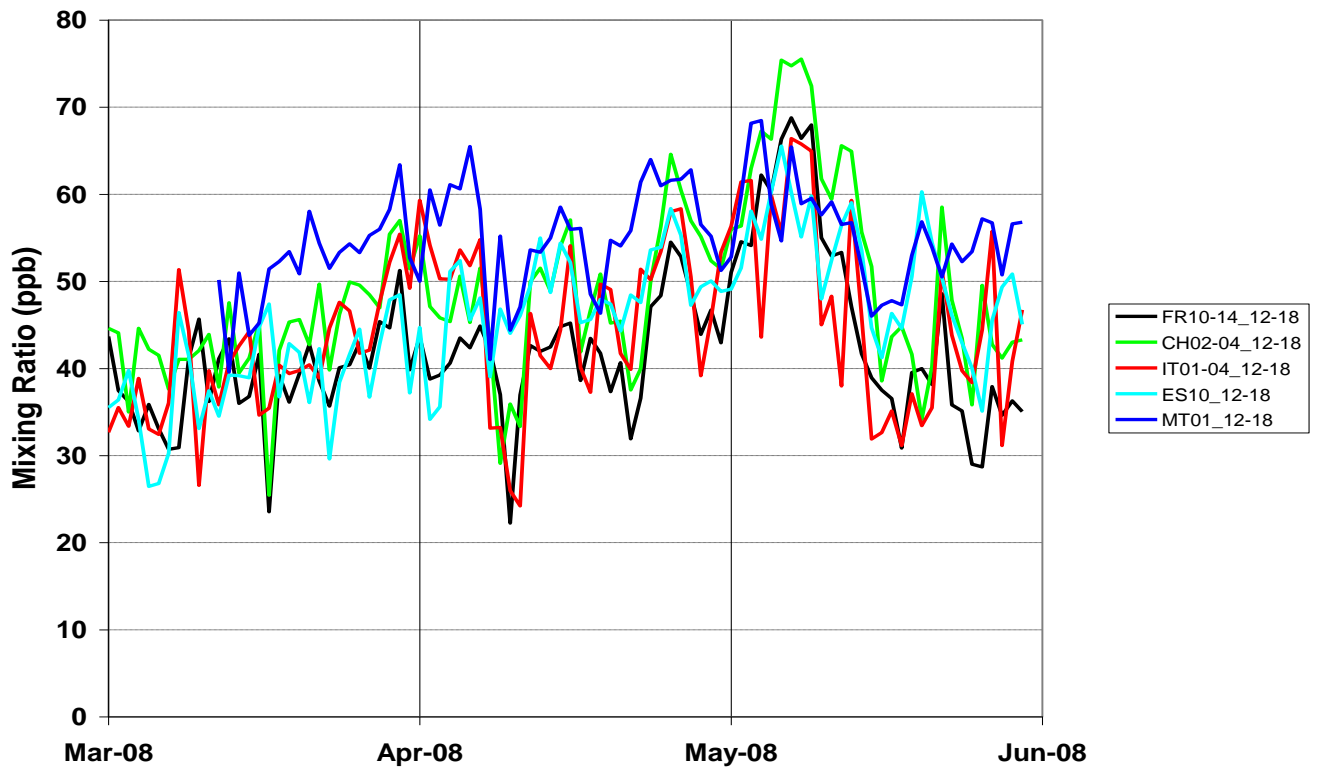
Figure 1:
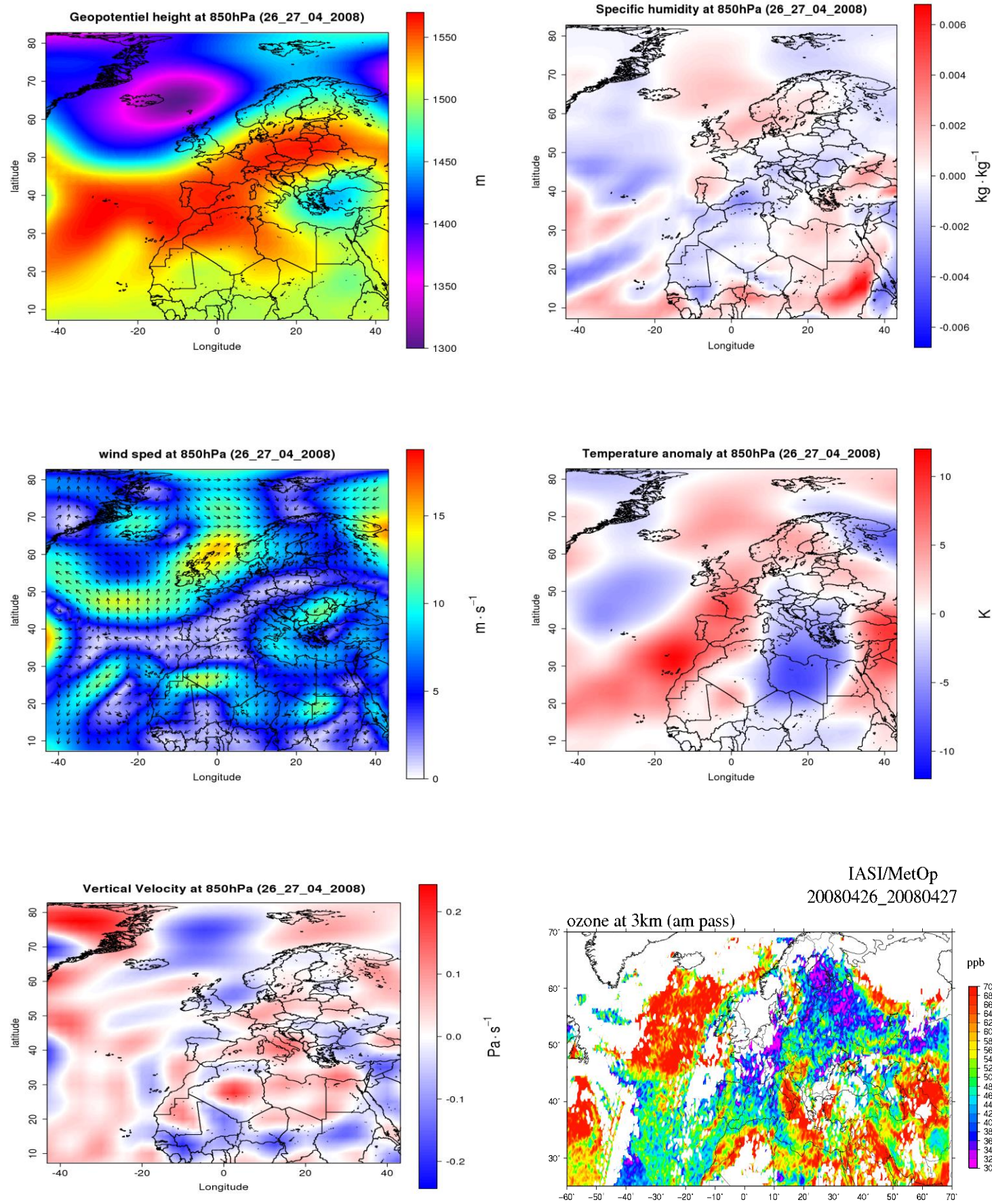
Figure 2:
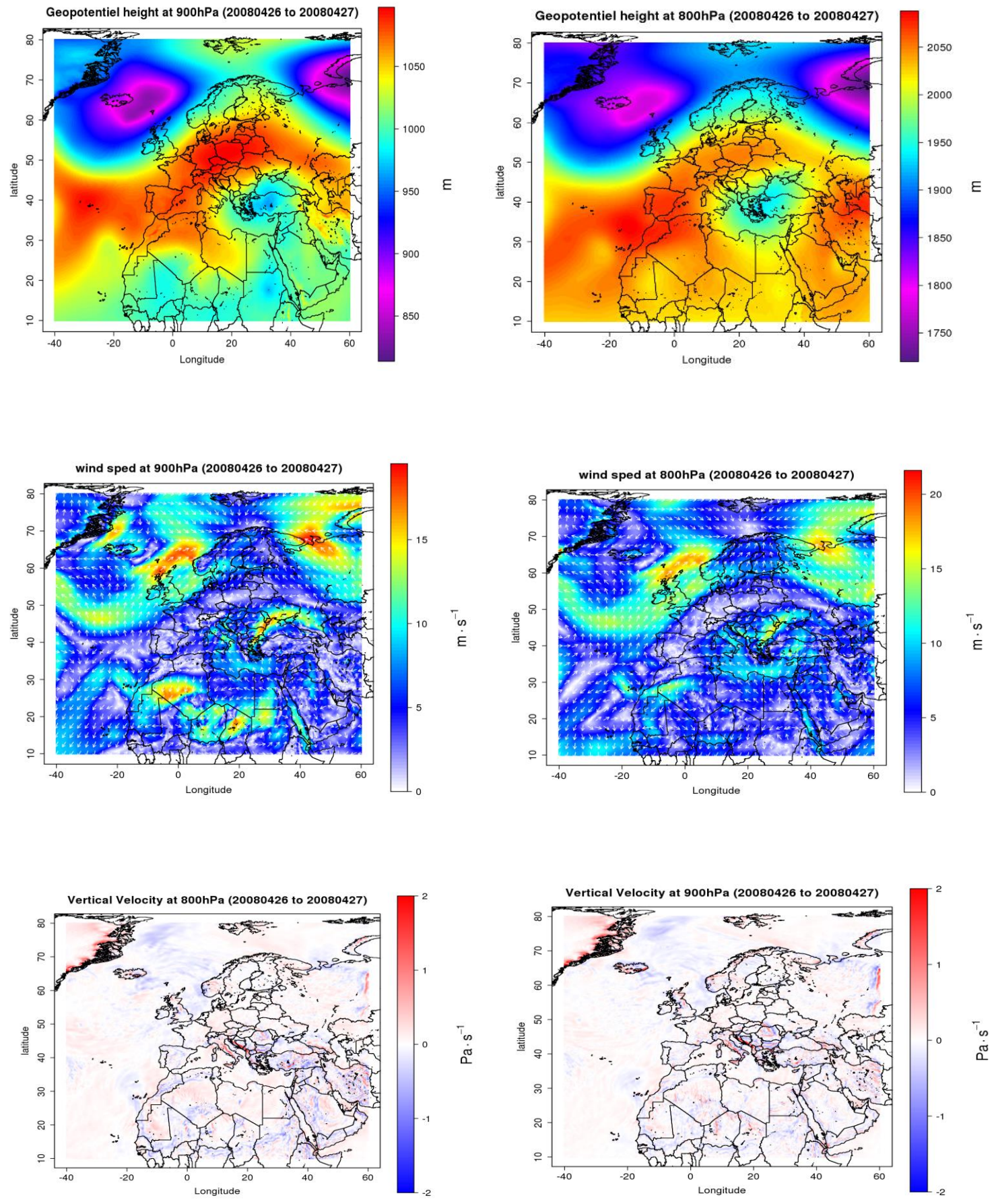
Figure 3:
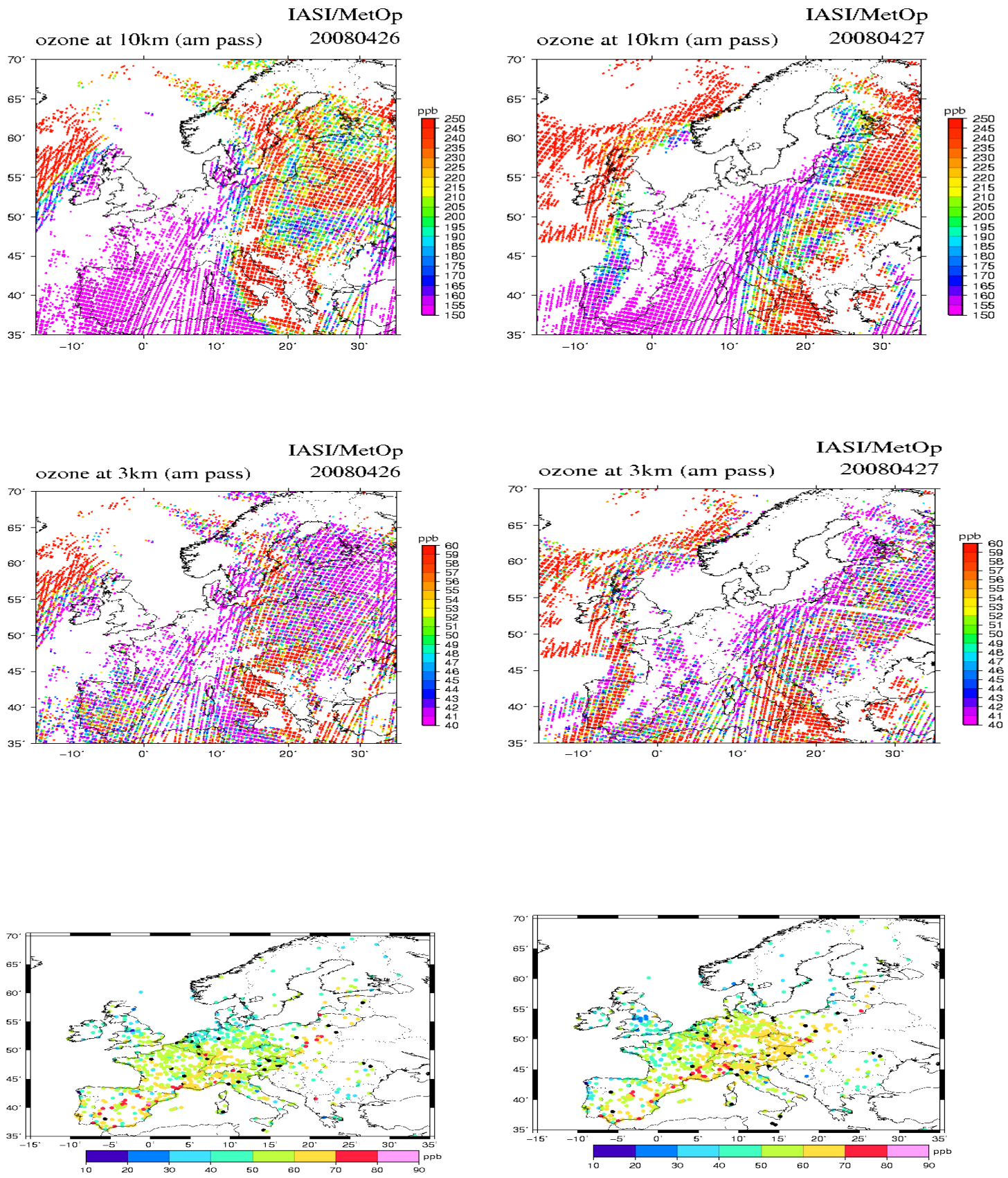
Figure 4:
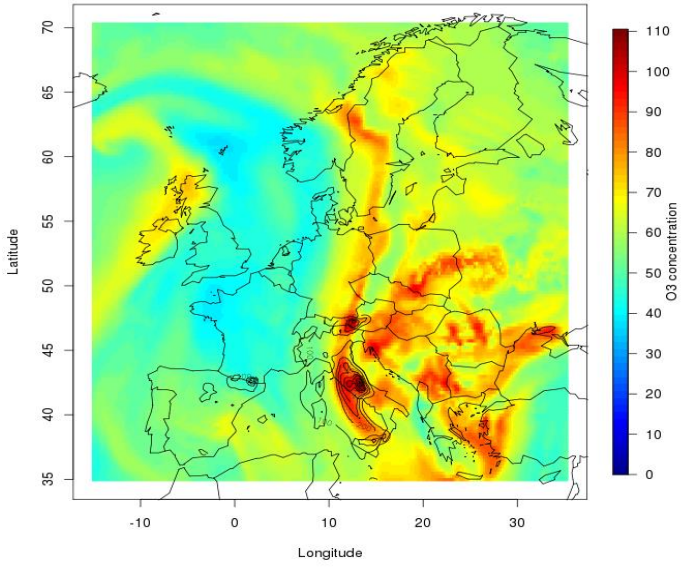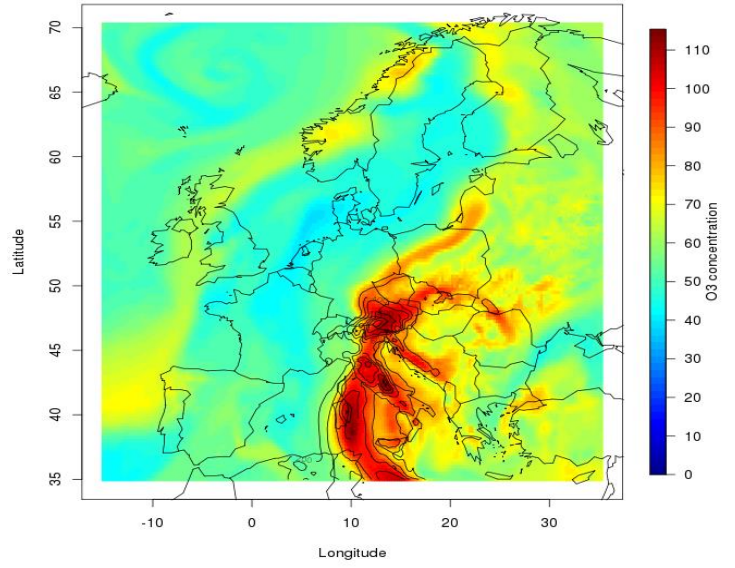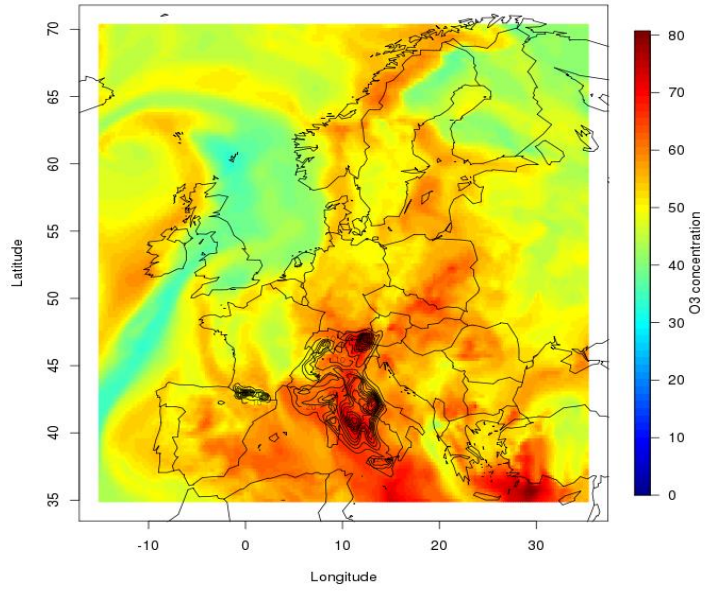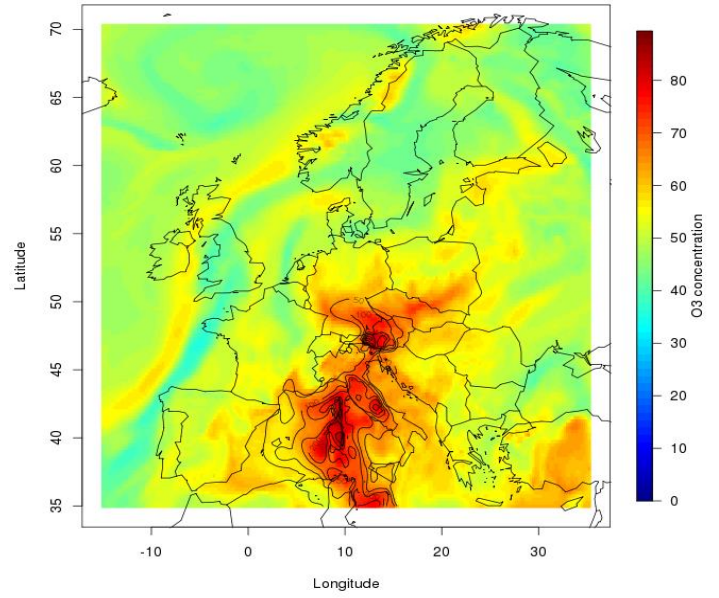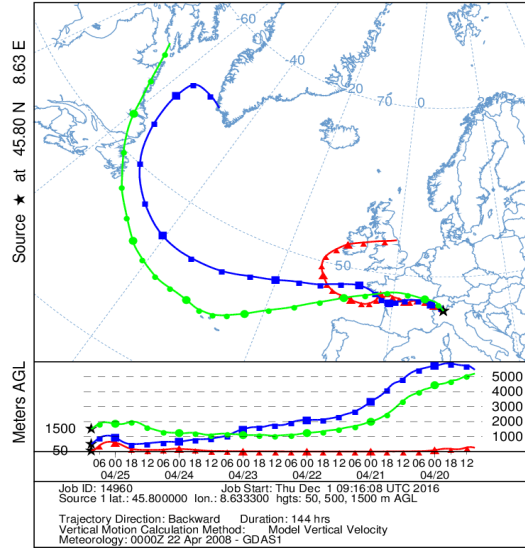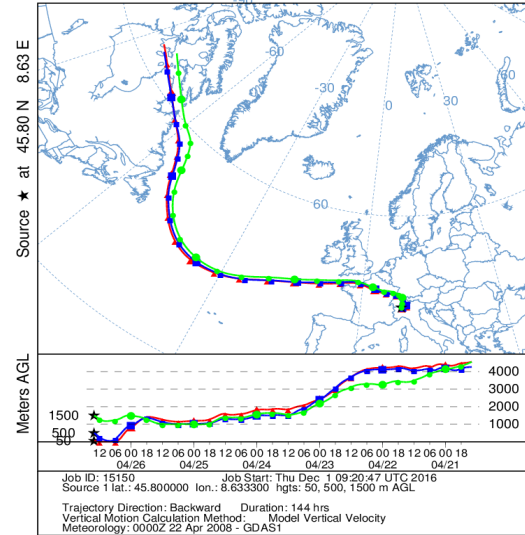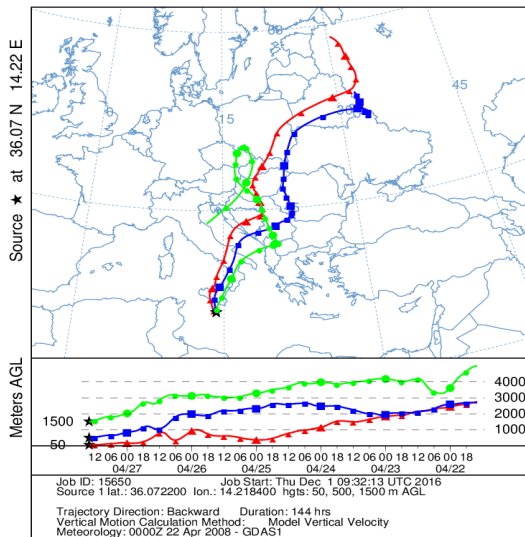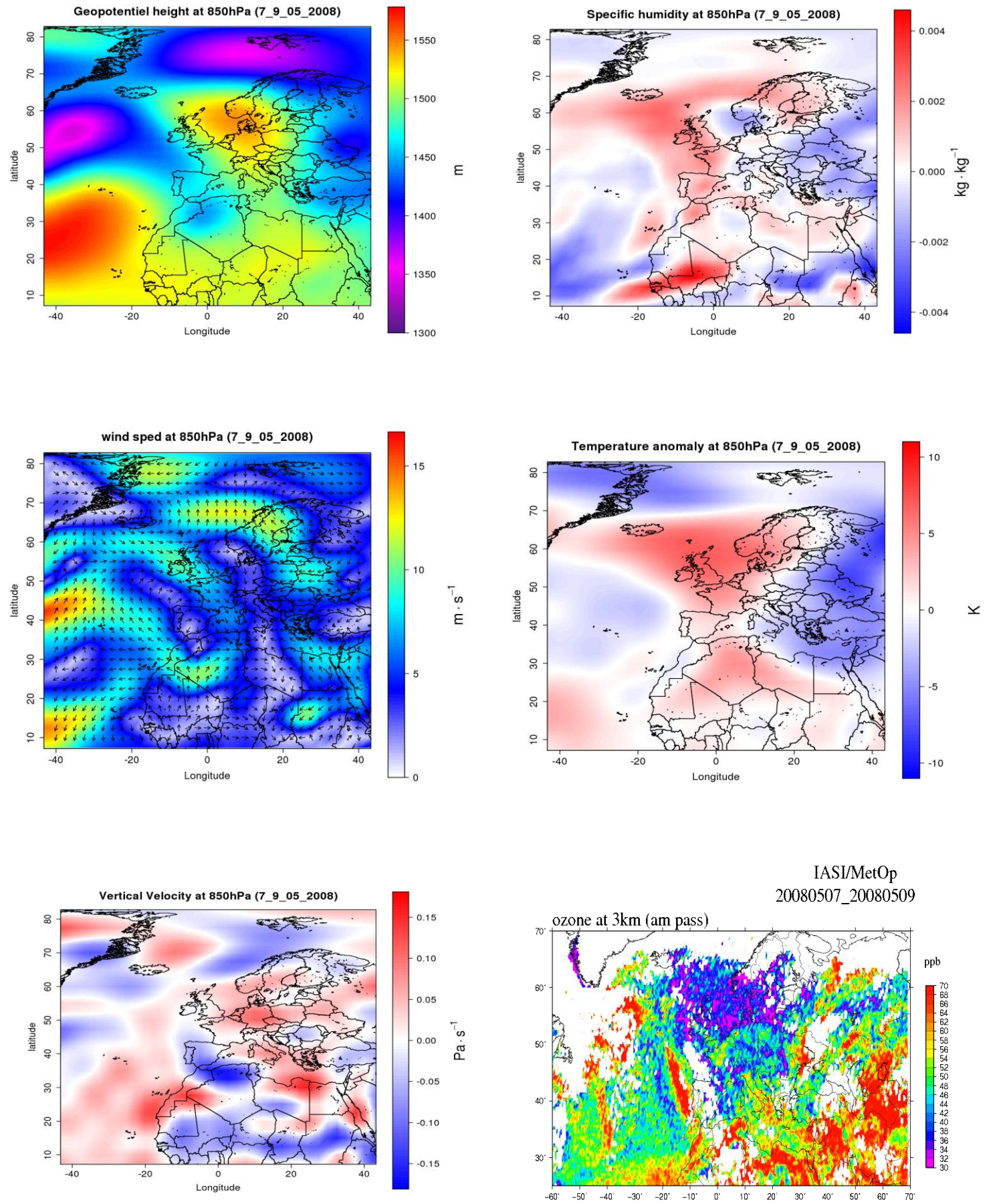
Figure 5

Figure 6:

Figure 7:

Figure 8:
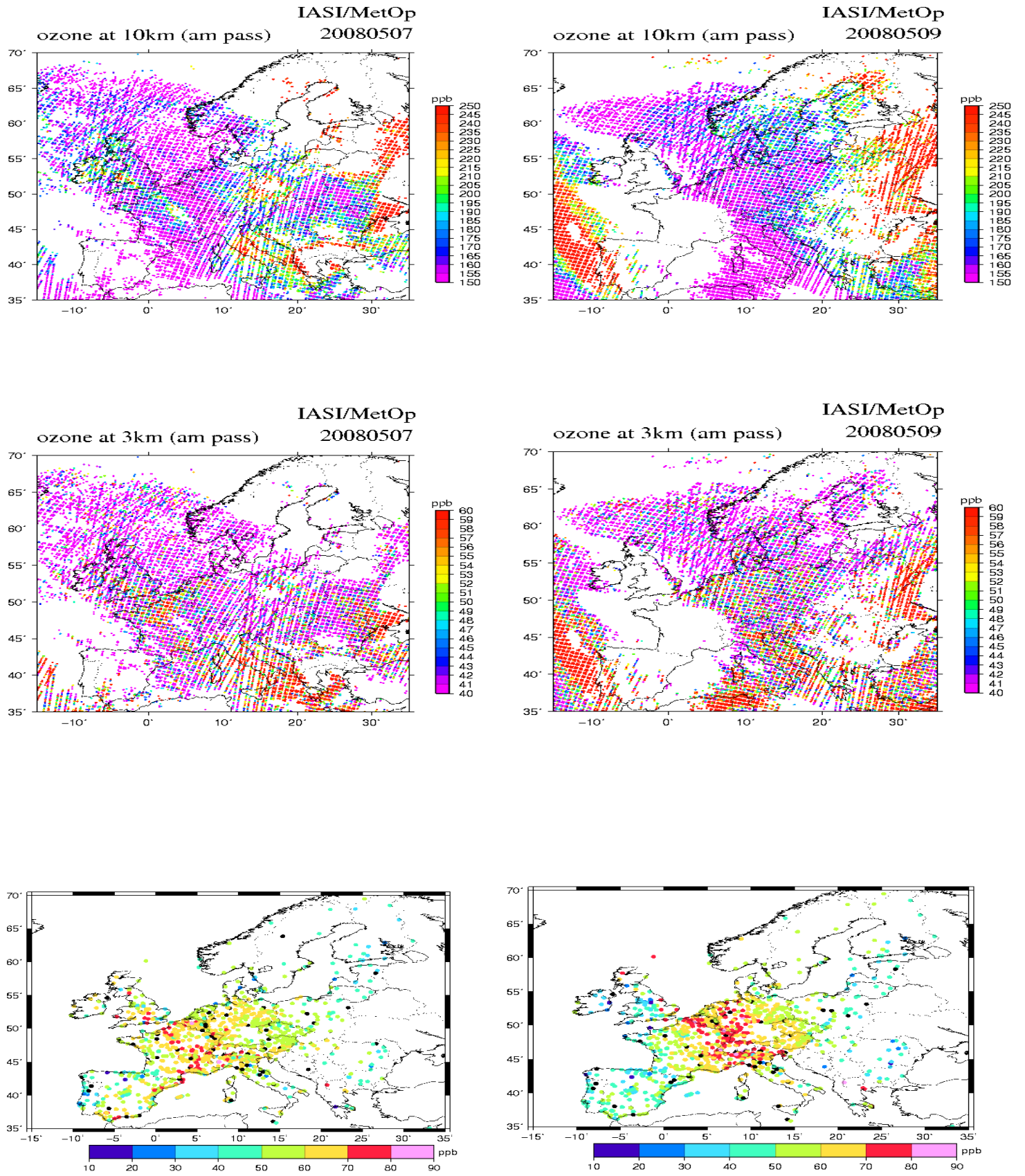
Figure 9:
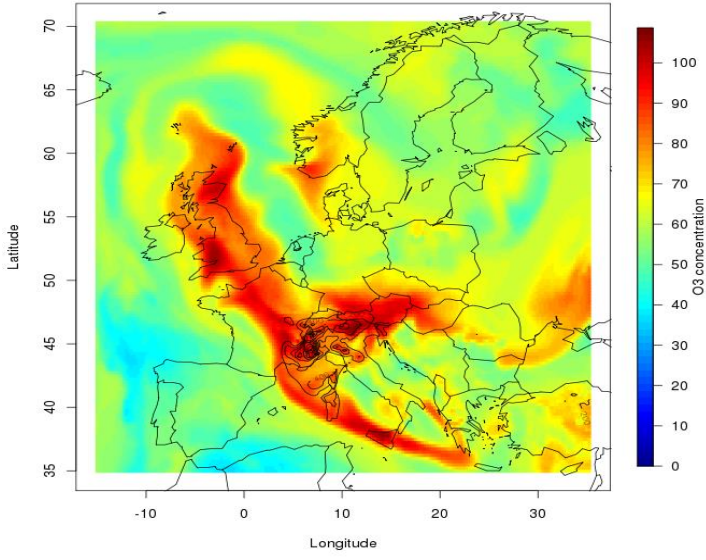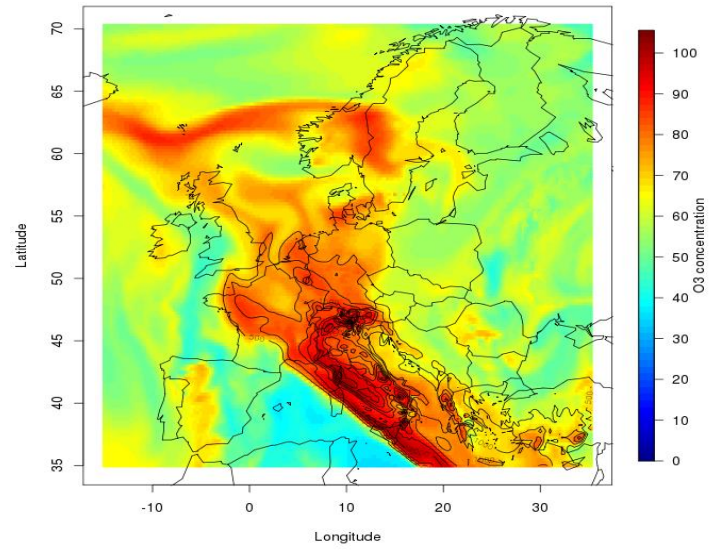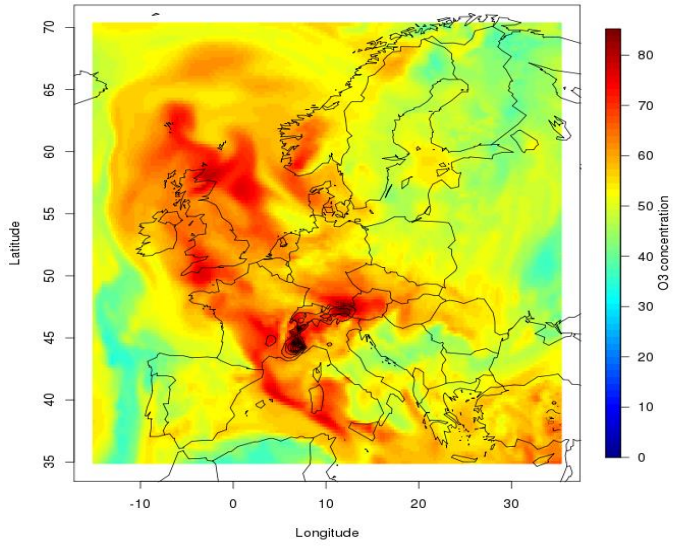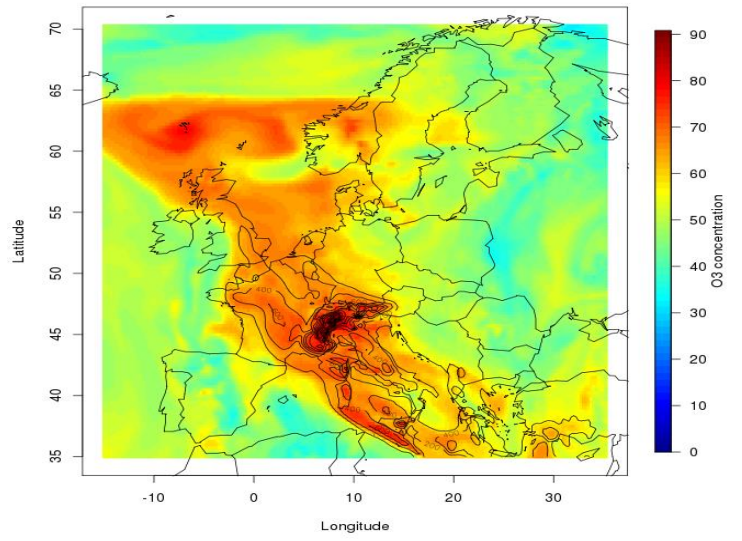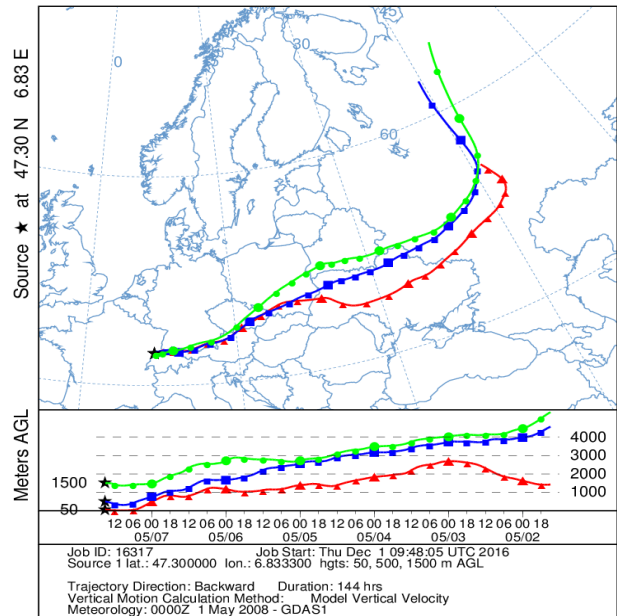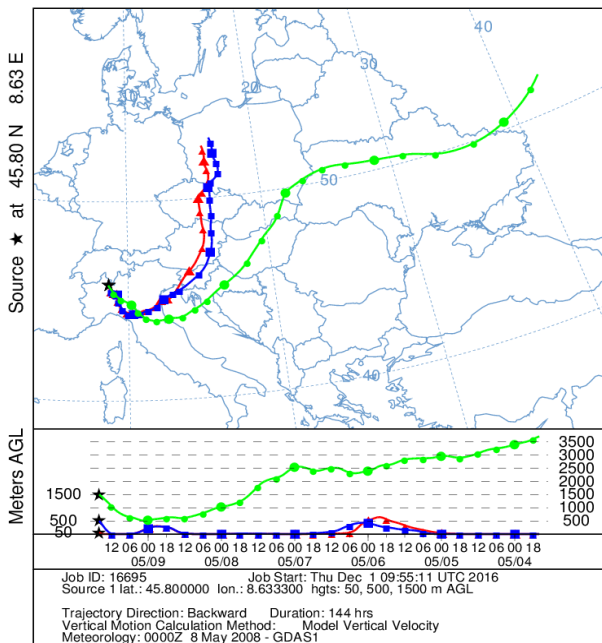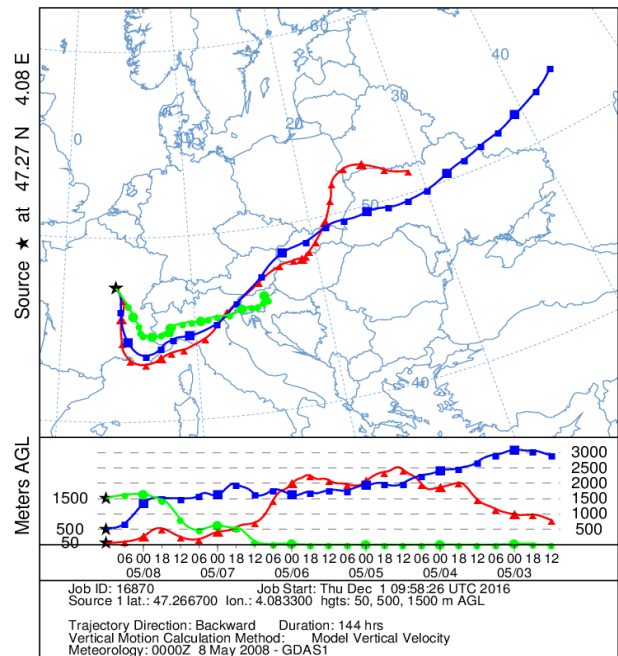
Figure 10

Figure 11

Figure 12:

Figure 13: